Annales Societatis Geologorum Poloniae (2025), vol. 95: ...–... https://doi.org/10.14241/asgp.2025.18

DEPOSITIONAL ENVIRONMENT, AGE AND GEOMORPHIC SIGNIFICANCE OF A PLEISTOCENE SPRING-RELATED CARBONATE COMPLEX, LIPTOV BASIN, CENTRAL WESTERN CARPATHIANS

Przemysław SALA[1] *, Pavel BELLA[2, 3], Michał GRADZIŃSKI[4], Pavel BOSÁK[5], Helena HERCMAN[6], Petr PRUNER[5], Stanislav ŠLECHTA[5], Ewa STWORZEWICZ[7] & Wojciech WRÓBLEWSKI[4]

[1] *Institute of Earth and Environmental Sciences, Nicolaus Copernicus University in Toruń, Lwowska 1, 87-100 Toruń, Poland; e-mail: p.sala@umk.pl*
[2] *Department of Geography, Faculty of Education, Catholic University in Ružomberok, Hrabovská cesta 1, 034 01 Ružomberok, Slovakia; e-mail: pavel.bella@ku.sk*
[3] *State Nature Conservancy of the Slovak Republic, Slovak Caves Administration, Hodžova 11, 031-01 Liptovský Mikuláš, Slovakia; e-mail: pavel.bella@ssj.sk*
[4] *Institute of Geological Sciences, Jagiellonian University, Gronostajowa 3a, 30-387 Kraków, Poland; e-mails: michal.gradzinski@uj.edu.pl, wojciech.wroblewski@uj.edu.pl*
[5] *Institute of Geology of the Czech Academy of Sciences, Rozvojová 269, 165 00 Praha 6, Czech Republic; e-mails: bosak@gli.cas.cz; pruner@gli.cas.cz; standa.slechta@atlas.cz*
[6] *Institute of Geological Sciences, Polish Academy of Sciences, Twarda 51-55, 00-818 Warsaw, Poland; e-mail: hhercman@twarda.pan.pl*
[7] *Institute of Systematics and Evolution of Animals, Polish Academy of Sciences, Sławkowska 17, 31-016 Kraków, Poland; e-mail: stworzewicz@isez.pan.krakow.pl*
** Corresponding author*

Sala, P., Bella, P., Gradziński, M., Bosák, P., Hercman, H., Pruner, P., Šlechta, S., Stworzewicz, E. & Wróblewski, W., 2025. Depositional environment, age and geomorphic significance of a Pleistocene spring-related carbonate complex, Liptov Basin, Central Western Carpathians. Annales Societatis Geologorum Poloniae, 95: xxx–xxx.

Abstract: The complex of freshwater carbonates at Čerená Hill in northern Slovakia was investigated. The facies recognised are mainly represented by a laminated crust, micritic limestone and phytoclastic boundstone and subordinately by moss boundstone and carbonate-siliciclastic mud. The alluvial sediments present at the base of the complex indicate that it was deposited within a flat stream valley at the foot of the Low Tatra Mts. The growth of the carbonates was controlled by the supply of deep-circulation water, containing geogenic CO_2, and its outflow to the marshy floodplain. This area was occasionally invaded by surface stream water, resulting in modification of the sedimentary facies, accompanied by a slight differentiation of the geochemical data ($\delta^{13}C$ values and $CaCO_3$ content). The U-series and palaeomagnetic data collectively show that the growth of the spring-related carbonate complex commenced between ca. 300 ka and persisted until 200 ka. Deposition during the warm interglacial phases of the Pleistocene is assumed; this is supported by the presence of a malacofauna assemblage, and a high contribution of calcified floral remains in a part of the studied sediments. Post-sedimentary modifications, mainly mass-wasting processes, resulting from the incision of adjacent valleys, shaped the area of Čerená Hill after it was cut off from a deep-water supply.

Key words: Travertine, tufa, deep-water circulation, lithofacies, palaeoenvironment.

Manuscript received 15 November 2025, accepted 23 December 2025

INTRODUCTION

Spring-related carbonates are widely distributed and occur on all of the continents except Antarctica (Pentecost, 1995; Ford and Pedley, 1996). They have been recognised in sediments ranging in age from deep time to recent (Brasier, 2011). However, because of their low fossilization potential, most spring-related carbonates are Quaternary in age. Such

carbonates are currently being formed at a very large number of sites in various environmental contexts.

Two categories of spring-related carbonates have been traditionally distinguished, namely tufa and travertine (see Jones and Renaut, 2010 and Sanders *et al*., 2011 for discussion on terminology). In general, deposits fed with ambient-temperature water and containing huge amounts of fossilised algae and macrophytes are classified as tufa (meteogene travertine *sensu* Pentecost, 2005), whereas those fed with thermal, highly mineralised water and containing scarce, if any, plant fossils are categorised as travertine (thermogene travertine *sensu* Pentecost, 2005). Both tufa and travertine have attracted considerable interest in recent years. The former has been studied intensively as a record of past environmental changes, the latter as a potential analogue of the enigmatic Cretaceous carbonates that serve as an economically important reservoir of hydrocarbons in the South Atlantic (e.g., Wright, 2012, 2022).

High numbers of tufa and travertine complexes in many regions of the world have been studied very thoroughly in different ways during the last thirty years. The facies variations and depositional systems of tufa and travertine have been recognised (Guo and Ridnig, 1998; Pedley, 2009; Gandin and Capezzuoli, 2014 and Pedley, 1990, 2009; Vázquez-Urbez *et al*., 2012, respectively). They were subsequently expanded and detailed in several regional case studies (e.g., travertine: Özkul *et al*., 2013; Gradziński *et al*., 2014a; Claes *et al*., 2015; Török *et al*., 2015, 2019; tufa: Gradziński *et al*., 2013; Arenas *et al*., 2014b; Toker, 2017). Simultaneously, in-depth analyses of contemporary tufa and travertine were supplemented by experimental works (e.g., Kele *et al*., 2008, 2011; Pedley *et al*., 2009; Gradziński, 2010; Shiraishi *et al*., 2010, 2020, 2022; Arenas *et al*., 2014a; Pedley, 2014; Słowakiewicz *et al*., 2023, 2024). As a result, a variety of interrelated factors controlling tufa and travertine growth, such as climatic conditions, water supply, hydrodynamic regime, seismotectonic activity, and the influence of microorganisms, was recognised.

It has also been noted that there are deposits resembling both tufa and travertine, situated between these two categories of spring-related carbonates. For simplicity, such deposits are referred to hereafter in this paper as hybrid spring-related carbonates. Until now, they have been named travertine (Özkul *et al*., 2014; Gradziński *et al*., 2015; Bisse *et al*., 2018; Luo *et al*., 2021) or tufa (Gradziński, 2010; Rodríguez-Berriguete and Alonso-Zarza, 2019; Rodríguez-Berriguete *et al*., 2022). Capezzuoli *et al*. (2014) proposed the term 'travitufa' to describe deposits with a chemical and isotopic signature, typical of travertine but displaying facies, typical of tufa. Mors *et al*. (2019) regarded travertine and tufa as two end members with several entities between them and provided a comprehensive description of the lateral transition from travertine to tufa in the modern and ancient deposits of the Argentinian Andes. In turn, Luo *et al*. (2021) noted the common occurrence of such sediments in fluvial systems and proposed the term "fluvial travertines" for them.

The formation of hybrid spring-related carbonates results from two processes. The decrease in water temperature with distance away from the feeding spring is the former (Guo and Riding, 1998). The latter takes place, when highly mineralised water of deep circulation is diluted by rainwater or surface stream water (Guo and Riding, 1998; Gradziński, 2010; Gradziński *et al*., 2015; Luo *et al*., 2021). Both processes commonly occur simultaneously, which results in the superimposition of their effects.

Hybrid spring-related carbonates are still poorly recognised, despite detailed descriptions of a few above-mentioned examples of recent and ancient sites. This scarcity distinguishes them from travertines and tufas, which have been the subject of many detailed studies. The existing knowledge gap can be bridged only by studying additional complexes of hybrid spring-related carbonates. Slovakia appears to be an excellent testing ground, since research conducted over the last 20 years has shown that many deposits, previously classified as travertine, actually display many characteristics typical of tufa. They have been classified as distal travertine by Gradziński *et al*. (2008) or travitufa by Pivko (2021).

The aim of this paper is to determine the facies and their spatial variation, depositional architecture, sedimentary environment and age, as well as the post-depositional history of the hybrid spring-related carbonates at Čerená Hill, northern Slovakia. These sediments were previously described as travertines (Ivan, 1943; Šubjak and Polášková, 1961; Kovanda, 1971; Vaškovský and Ložek, 1972; Vaškovský, 1980), but preliminary studies by the authors (e.g., Sala, 2016) and observations by Pivko (2021) and Pivko and Vojtko (2021) have shown that they share facies characteristics with tufa.

GEOLOGICAL SETTING

The Central Western Carpathians include mountain chains, composed predominantly of sedimentary rocks, partly carbonates of Mesozoic age (Maheľ and Buday, 1968). The sedimentary rocks cover an older, crystalline basement, which constitutes the cores of many mountain massifs. All the rocks in question were deformed in Late Cretaceous time, with several nappes formed and pushed to the north as an effect of crustal shortening caused by the convergence of Adria-Africa and Europe (Plašienka, 2008, 2018). The Central Western Carpathians were subject to erosion and denudation during the Paleocene to Early Eocene. Subsequently, tectonic subsidence created the Central Carpathian Palaeogene Basin, filled with the deposits of a marine transgression of Eocene–Oligocene (Early Miocene?) age (Soták, 1998). A sequence, comprising conglomerates, limestones and a thick flysch-type package, was laid down. This sequence is called the Central Carpathian Palaeogene.

Shaping of the modern relief of the Central Western Carpathians started in Miocene time and was a result of tectonic activity in the region. In the Oligocene–Early Miocene, some parts of the region started to be uplifted and exhumed in a transpressional regime (Králiková *et al*., 2014; Anczkiewicz *et al*., 2015 and references therein). The Central Carpathian Palaeogene rocks were eroded from uplifted parts, which presently form mountain massifs, composed of Mesozoic rocks and their crystalline basement. The neighbouring intramontane basins of the tectonic depressions are still filled with the Central Carpathian Palaeogene rocks, predominantly carbonate-poor flysch sandstones and

mudstones (Fig. 1). The individual massifs have been uplifted and exhumed to different extents. Surface fluvial drainage systems were created. Simultaneously, springs along deep-seated faults started to expel deeply circulating water, highly charged with CO_2 of crustal or even mantle origin. Travertine was deposited near the springs. Such springs and gas vents are now common throughout the Central Western Carpathians (Hynie, 1963; Cornides and Kecskés, 1982; Povinec *et al*., 2010; Wróblewski *et al*., 2024). The springs are commonly associated with recent travertine precipitation (Kovanda, 1971; Gradziński, 2010; Gradziński *et al*., 2015; Pivko, 2021; Pivko and Vojtko, 2021).

The Liptov Basin is one of the tectonic depressions, located in the Central Western Carpathians (Fig. 1). The Choč Mts and Tatra Mts limit the basin from the north, and the Low Tatra Mts from the south. Quaternary sediments directly overlie siliciclastic rocks of Palaeogene age, mostly claystones of the Huty Formation and flysch-like deposits of the Zuberec Formation. They represent fluvial and alluvial/colluvial deposits; the former consist of several generations of river terraces (e.g., Droppa, 1964, 1972; Vaškovský, 1980; Vitovič and Minár, 2018; Vitovič *et al*., 2021, 2022).

The Liptov Basin contains abundant deposits of travertine, both fossil and modern (Kovanda, 1971; see also Fig. 1). They are aligned along faults, bounding and crossing the basin. The travertine sites in the northwestern part of the basin, namely at Bešeňová and Lúčky, are more well known (Gradziński, 2010; Gradziński *et al*., 2015; Słowakiewicz *et al*., 2023, 2024; Vieira *et al*., 2023); some of them are also tourist attractions. However, less is known about the travertines, located in the southern part of the basin. The most important travertine sites there include Liptovský Ján, Liptovské Sliače, and Čerená Hill, known also under the name Ludrová, after the neighbouring village (Kovanda, 1971; Gradziński *et al*., 2018; Pivko, 2021).

Čerená Hill forms an elongated flat-topped plateau, reaching nearly 600 m longitudinally in a north-south direction and approximately 150 m in width, with an area of more than 0.25 km^2. Its top is located at ca. 646 m a.s.l. (Fig. 2). The hill is composed of cemented gravels, capped by a carbonate complex, the thickness of which is estimated to be 20–21 m (Šubjak and Polášková, 1961). The carbonate was penetrated by numerous drill holes, which reached cemented gravel at its basement. Following the opinion by Šubjak and Polášková (1961), the Čerená carbonate was classified as a travertine mound ('travertinová kupa' of Kovanda, 1971; 'kopa' of Droppa, 1972), spring mound or fen (Pivko and Vojtko, 2021). The travertine and underlying cemented gravel were laid down on an erosional surface of Palaeogene rocks. The presence of W–E- and NNW–SSE-trending faults is assumed below Čerená Hill (Gross *et al*., 1979), which determines the outflow of mineralised water to the surface.

MATERIALS AND METHODS

Fieldwork and petrography

Four logs were measured bed-by-bed in the northern part of the quarry at Čerená Hill (Figs 2, 3). During the field surveys, 56 hand specimens were collected. The calcium carbonate content was measured in each of them, using an Ejkelcamp calcimeter, following the Scheibler method. Microfacies analysis was conducted in 25 thin sections under a standard petrographic microscope. Petrographic types of sediments were classified with reference to the concept, proposed by Della Porta (2015). A scanning electron microscopy (SEM) Hitachi S-4700 Microscope, equipped with a NORAN Vantage energy dispersive spectrometer (EDS), was used to observe 12 gold-covered samples; three of them were etched previously in 2% hydrochloric acid for one minute. All the above laboratory work was carried out in the Institute of Geological Sciences, Jagiellonian University in Kraków.

X-ray diffraction

The mineral composition of two bulk samples was determined by means of X-ray diffraction, using a standard procedure. Furthermore, the clay fraction (<2 μm) was separated from one sample, following the procedure proposed by Jackson (1969) to remove carbonate minerals, organic matter, and the amorphous phase of iron and manganese compounds. Subsequently, the retrieved material was saturated with calcium ions and subjected to dialysis for the removal of chlorides. The separation of the clay fraction was performed by centrifugation. The measurements were conducted in air-dried (AD) conditions, after ethylene glycol saturation (ED), and after heating for at least 1 h at 550 °C (HT). Analyses were conducted at the Institute of Geological Sciences, Jagiellonian University in Kraków, using an XPert APD Philips diffractometer, equipped with a PW 3830 generator and a PW 3020 goniometer. CuKα radiation was used with an applied voltage of 40 kV and a current of 30 mA. A ClayLab Computer program (Mystkowski, 1999), supported by the description given by Środoń (2006), was used to identify the clay minerals.

Stable isotope analyses

Oxygen and carbon isotopic composition was measured in 28 samples at the Stable Isotope Laboratory (ISOLAB) of the Institute of Geological Sciences, Polish Academy of Sciences (Warsaw, Poland). Samples were dissolved in 100% phosphoric acid at a temperature of 70 °C, using Kiel IV apparatus. Measurements were made in a Thermo-Finnigan Delta Plus Mass Spectrometer. The values of $\delta^{13}C$ and $\delta^{18}O$ are presented with reference to the V-PDB standard. The standard deviation for isotope analysis was established as ±0.03‰ for $\delta^{13}C$ and ±0.07‰ for $\delta^{18}O$.

Malacological investigation

Mollusc shells were collected during fieldwork in a twofold manner. Firstly, eleven samples of loose material with a weight between 1.2 and 1.8 kg were collected from poorly cemented travertine layers. They were subsequently rinsed on sieves (mesh size <1 mm) under running water, and the shell material was picked out. Secondly, single shells were also taken selectively from the better-cemented layers, directly at the outcrop.

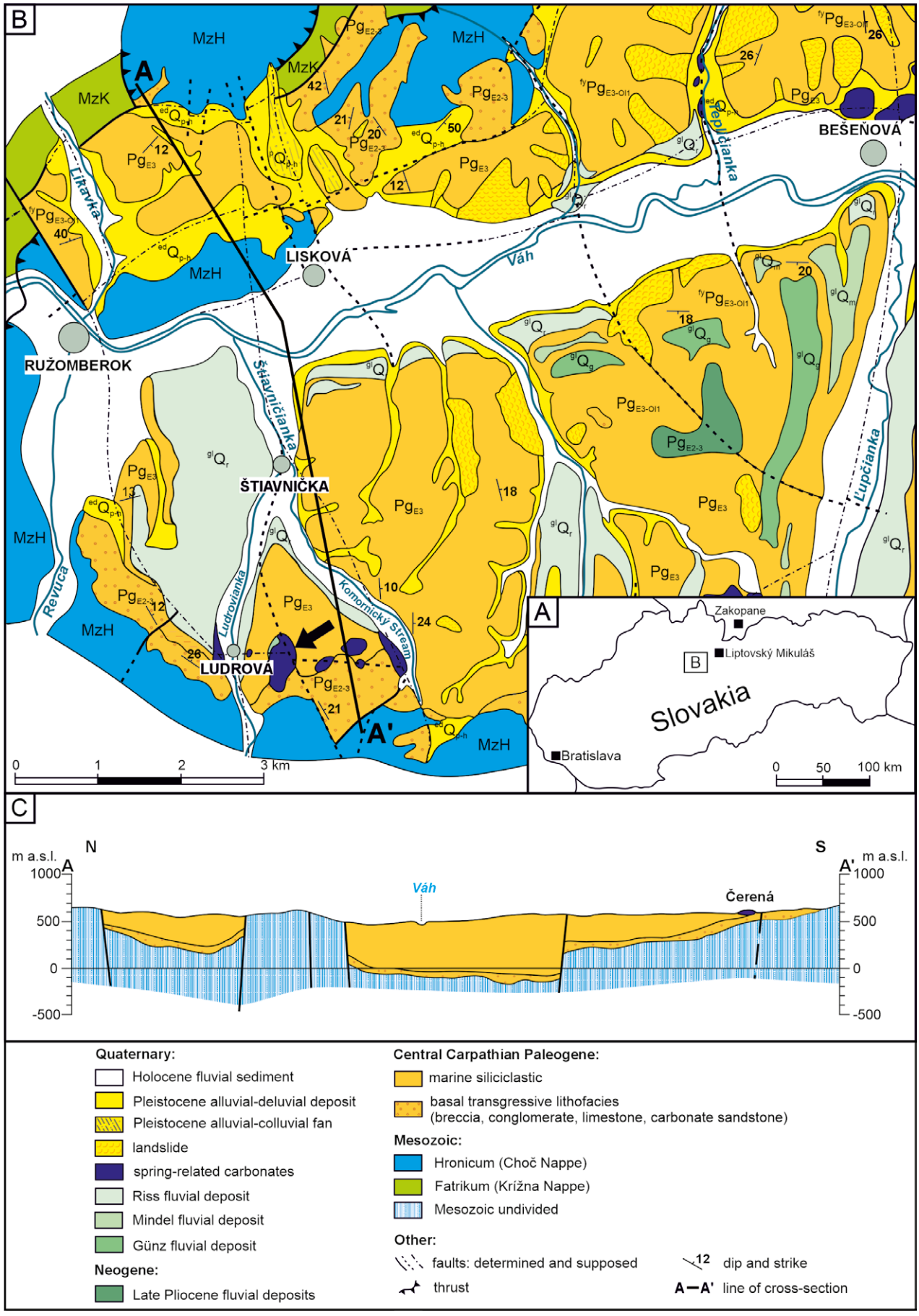

Fig. 1. Location and geological setting of Čerená Hill and its surroundings. **A.** Location of the area in Slovakia is presented on inset B. **B.** Lithostratigraphic map of the western part of the Liptov Basin. Arrow indicates the spring-related carbonates at Čerená Hill **C.** Cross-section along the line A–A'. B and C based on Gross *et al*. (1979, 1980, 1984) and Vitovič (2020), modified.

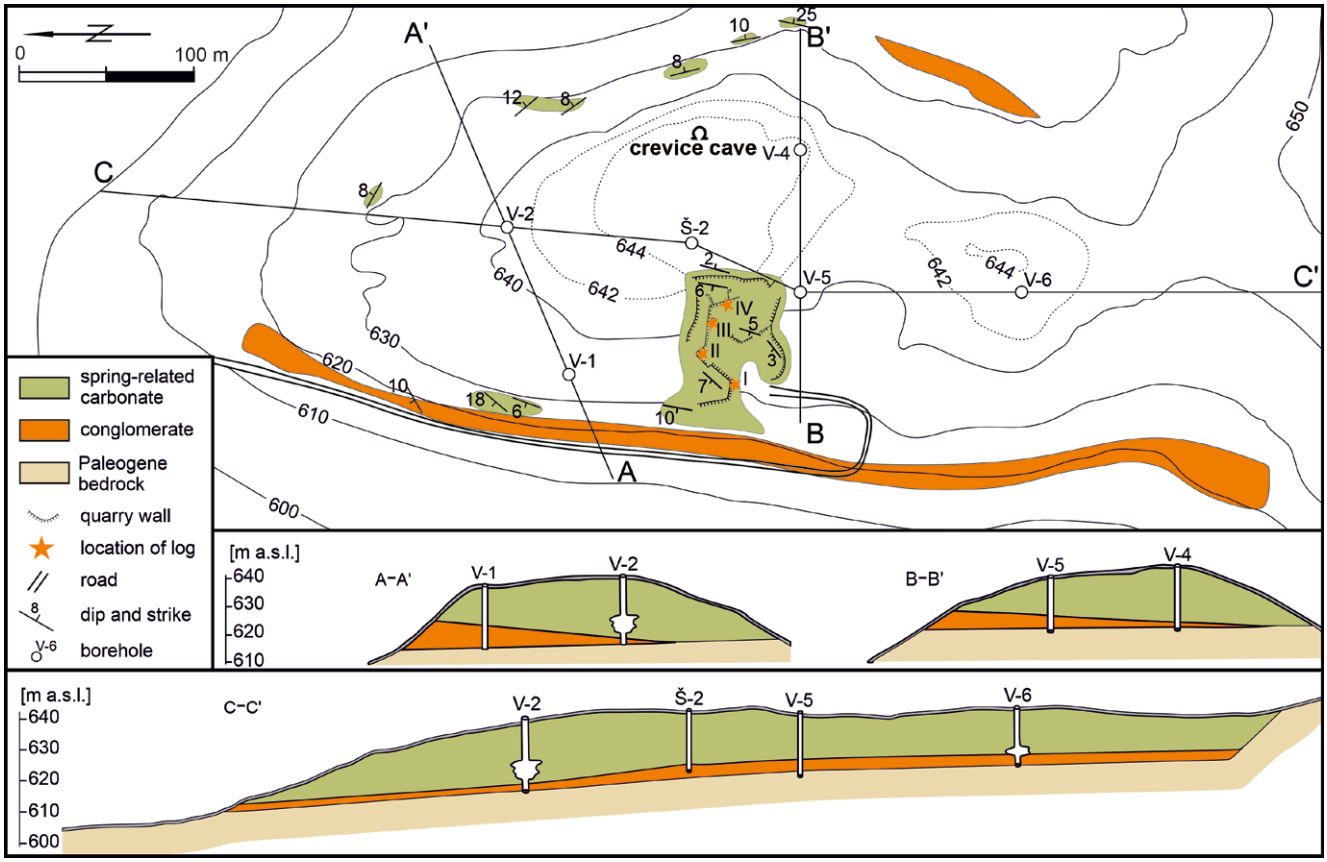

Fig. 2. Sketch map of Čerená Hill with longitudinal and transverse cross-sections (based on Droppa, 1972).

U-series dating

At the first stage of the work, four samples were analysed, using alpha spectrometry by a U and Th isotopic composition measurement method at the Uranium-Series Laboratory (LUT) of the Institute of Geological Sciences, Polish Academy of Sciences (Warsaw, Poland). The standard chemical procedure of uranium and thorium separation from calcite (Ivanovich and Harmon, 1992) was applied. Samples selected for U-series analyses were cleaned of visible contamination, crushed, and then washed several times in an ultrasonic bath. The samples (1–10 g) were dissolved in 6 M nitric acid, and uranium and thorium were separated by a chromatographic method, using a DOWEX 1x8 ion exchanger. The efficiency of chemical separation was controlled through the addition of a ^{228}Th-^{232}U spike (UDP10030 tracer solution by Isotrac, AEA Technology) before chemical treatment. Activities measurements (α spectrometry) were obtained on the ALPHA ENSEMBLE spectrometer, made by the EG&G ORTEC company. Alpha particle spectra analyses and age calculation were performed, using "URANOTHOR 2.6" software. Each spectrum was corrected for background and the delay time between chemical separation and measurement.

The second stage of the work included the U-series dating of two samples, analysed previously by the palaeomagnetic method. Calcite samples (ca. of 0.3 g) were drilled from parts of the samples with no visible secondary alteration or porosity and minimal detrital contamination. Chemical separation of uranium and thorium from the carbonate matrix was done at the Uranium-Series Laboratory (LUT) of the Institute of Geological Sciences, Polish Academy of Sciences (Warsaw, Poland). After the thermal decomposition of organic matter, a ^{233}U-^{236}U-^{229}Th mixture was added to the samples before further chemical treatment. The calcite samples were then dissolved in nitric acid. Uranium and thorium were separated from the carbonate matrix, using the chromatographic method with TRU Resin. Internal standard, and blank samples were prepared and processed in parallel to all series of studied samples. The isotopic composition of U and Th was measured at the Institute of Geology of the Czech Academy of Sciences (Prague, Czech Republic). Measurements were performed with a double-focusing sector-field ICP mass analyser (Element 2, Thermo Finnigan MAT). The instrument was operated at a low mass resolution ($m/\Delta m \geq 300$). Measurement results were corrected for background count and chemical blanks. The final results are reported as activity ratios.

U-series ages were iteratively calculated from the ^{230}Th/^{234}U and ^{234}U/^{238}U activity ratios, using following decay constants (in yr^{-1}): $\lambda^{238} = (1.55125 \pm 0.0017)\cdot10^{-10}$ (Jaffey *et al.*, 1971), $\lambda^{234} = (2.826 \pm 0.0056)\,10^{-6}$ (Cheng *et al.*, 2000), $\lambda^{232} = (4.95 \pm 0.035)\cdot10^{-11}$ (Holden, 1990), $\lambda^{230} = (9.1577 \pm 0.028)\cdot10^{-6}$ (Cheng *et al.*, 2000). All uncertainties were evaluated and taken into account, when assessing age uncertainty, using error propagation rules. For samples measured by alpha spectrometry, the quoted errors are 1σ; for samples measured by mass spectrometry, the errors are 2σ.

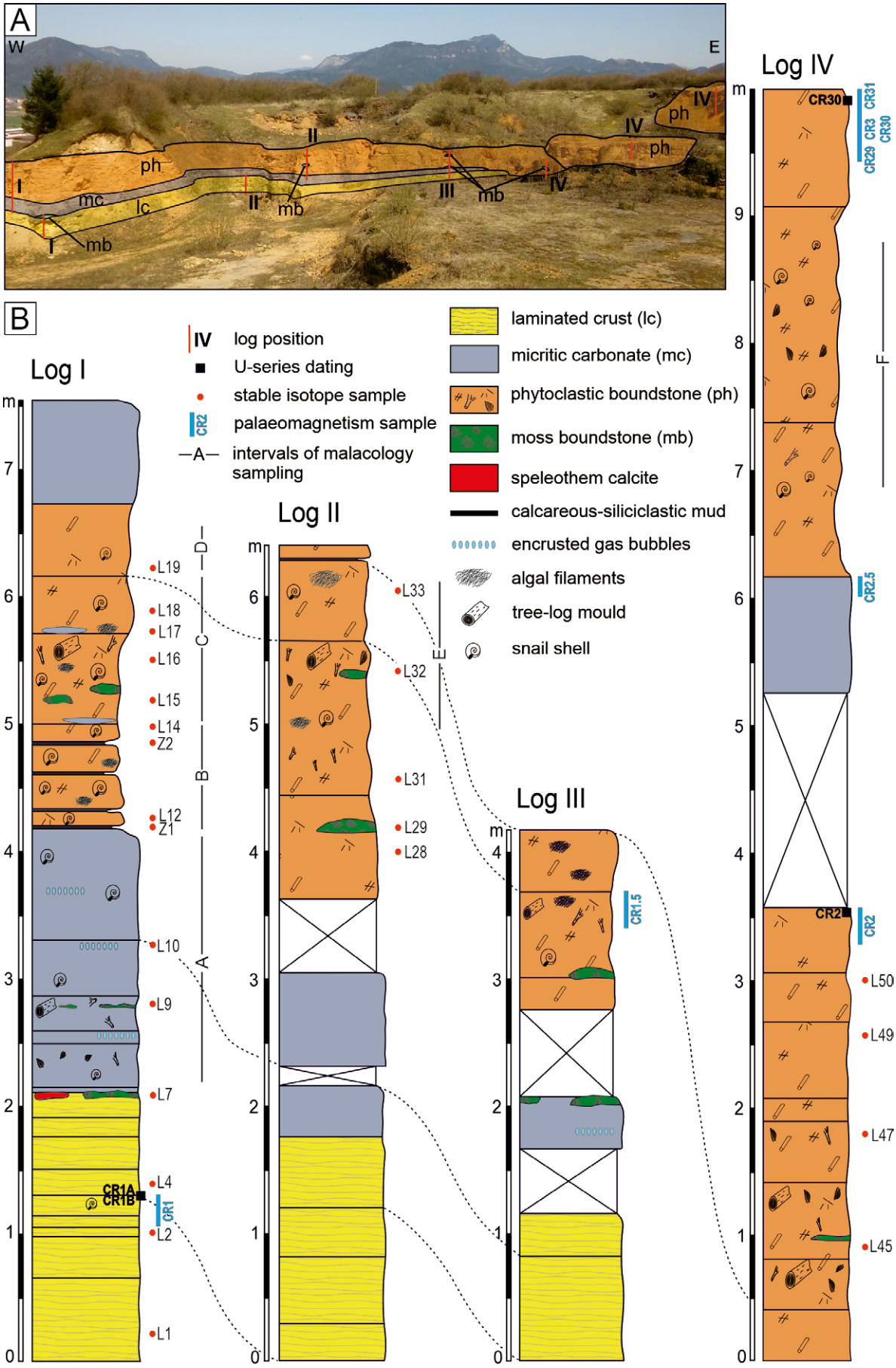

Fig. 3. Lithofacies distribution in the quarry at Čerená Hill. **A.** Overview of the northern part of the quarry. Colour shades reflect the facies distribution (for description, see legend in B). Red lines indicate the locations of logs. **B.** Lithological logs. Dashed lines show the correlation of the logs.

Palaeomagnetic analyses

Palaeomagnetic analyses were based on the 7 drill cores, with 33 samples and 83 measurements. The natural remanent magnetization (NRM) of the rocks was measured on a Liquid helium-free Superconducting Rock Magnetometer (type 755 4K SRM), and the volume magnetic susceptibility (MS) of the samples was measured on the KLY-4 Kappabridge (Jelínek, 1966, 1973). In order to resolve the NRM components, the latter equipment was used, with alternating field demagnetisation (AF) up to the peak field of 100 mT, whereas the former was mostly combined with the thermal demagnetisation (TD) in the field-free space, produced by the MAVACS equipment. The ambient magnetic field in the cooling chamber of the MAVACS demagnetiser did not exceed 1 nT, owing to a built-in rotating-coil magnetometer, controlling the currents in its Helmholtz coil system (Příhoda *et al.*, 1989). The characteristic remanent magnetization (ChRM) of each sample was determined by subjecting its demagnetisation results to the principal component analysis technique of Kirschvink (1980) and the Remasoft 3 software (Chadima and Hrouda, 2006). Palaeomagnetic analyses were completed in the Department of Palaeomagnetism, Institute of Geology of the Czech Academy of Sciences in Průhonice (for the complete procedure description, see: Zupan Hajna *et al.*, 2008).

Two pilot samples were subjected to the analysis of isothermal remanent magnetisation (IRM) acquisition and AF demagnetisation curves, with the aim of establishing the magnetic hardness of the magnetically active minerals contained in the sediments. The IRM was progressively acquired, using a Magnetic Measurements MMPM10 pulse magnetizer in fields of up to 1 T. The acquired IRM was measured after each imparted field with an AGICO JR-5 spinner magnetometer.

SEDIMENTARY FACIES – DESCRIPTION AND INTERPRETATION

Conglomerate

Description

The conglomerate extends laterally throughout Čerená Hill and discordantly overlies Palaeogene marine rocks. Its base is not exposed at present; the maximal thickness reaches ca. 2 m and slightly increases towards the northwest (Droppa, 1972). The conglomerate is capped by travertines.

The deposits of this facies are clast-supported pebble gravel, with an admixture of granules and cobbles (D_{max} = 25 cm; Fig. 4A). The framework is mostly composed of poorly sorted and subrounded pebbles of Middle Triassic limestones and dolostones, as well as Palaeogene sandstones (Droppa, 1972). At many places, the clasts are imbricated, while their longer axes align in a NW–SE direction. The facies has a fine-grained matrix but locally exhibits an openwork texture. Primary porosity is filled with calcite sparite or micrite. The measured calcium carbonate content in the cement of the conglomerates ranges from 75 to 80%. The $\delta^{13}C$ value of the cement is –5.03‰, whereas the $\delta^{18}O$ value is –7.08‰ (Tab. 1).

Interpretation

The conglomerate is attributed to fluvial bedload transport from the southeast, as indicated by clast imbrication. This suggests that the uplifted Low Tatra Mts acted as

Table 1

Stable isotopic composition ($\delta^{13}C$ and $\delta^{18}O$) of analysed samples (see Figure 3 for sample locations).

Sample no.	Lithofacies	$\delta^{13}C$ (‰ V–PDB)	$\delta^{18}O$ (‰ V–PDB)
C5	SP	2.77	–7.63
L0	CO	–5.03	–7.08
L1	LC	5.02	–8.62
L2	LC	4.59	–10.13
L4	LC	4.29	–9.10
L7	MB	3.70	–8.13
L9	MC	3.94	–8.62
L10	MC	3.68	–8.82
L12	PH	3.02	–8.90
L14	PH	5.24	–9.84
L15	MB	3.32	–8.58
L16	PH	3.18	–8.57
L17	MC	4.40	–8.44
L18	PH	3.01	–8.45
L19	PH	3.54	–8.23
L28	PH	3.83	–8.76
L29	MB	4.20	–8.74
L31	PH	3.62	–8.47
L32	PH	3.41	–8.42
L33	PH	3.92	–8.15
L45	PH	3.83	–8.15
L47	PH	4.11	–8.35
L49	PH	3.08	–8.44
L50	PH	4.04	–8.13
Z1	CM	3.42	–8.75
Z1–2	CM	3.37	–9.02
Z2	CM	2.67	–8.49
Z2–2	CM	2.22	–8.69

* Lithofacies: CO – conglomerates; LC – laminated crust; MC – micritic carbonate; PH – phytoclastic boundstone; MB – moss boundstone; CM – calcareous-siliciclastic mud; SP – speleothem calcite.

the alimentation area, which is consistent with the present-day local topography and the petrographic composition of the clasts. The conglomerate is considered to be the deposits of a stream-dominated alluvial fan (*sensu* Collinson, 1986). Cementation of some parts of the alluvial fan proceeded under the influence of water that formed spring-related carbonates on the surface (see Gradziński *et al*., 2014b; Wang *et al*., 2016; Rodríguez-Berriguete *et al*., 2017).

Laminated crust

Description

The laminated crust is composed of strongly cemented, beige to grey carbonate, the peculiar feature of which is slightly undulated, thin layers, often separated by elongated pores (Fig. 4B). The laminated crust dips towards the west or northwest at an angle of up to 10°. The facies occurs at the base of the carbonate complex, resting directly on the conglomerate. It extends laterally throughout the whole quarry; it also builds small, isolated outcrops on the slopes of Čerená Hill (Fig. 2).

Two lithotypes compose the facies, namely: (i) laminated sparite/microsparite cementstone, and (ii) peloidal grainstone. The laminated sparite/microsparite cementstone predominates (Fig. 4C, D). Sparitic laminae are composed of a mosaic of isometric or rhombohedral crystals, although vertically oriented, fan-like crystals were also observed. Microscopic examination revealed thin, up to 0.1 mm, dense micritic laminae , which are slightly undulating and parallel to the facies layering. Empty moulds after cyanobacteria encrusted by calcite occur, though they are relatively uncommon (Fig. 4E). They are a few micrometres in width. Peloids of various sizes, up to 2 mm in width, cemented by sparite, locally form peloidal grainstone (Fig. 4F). Some peloids are aggregates of smaller micrite grains, displaying ovate shapes. The peloids are cemented by mosaic or bladed sparite.

Sparse quartz grains and muscovite flakes are the only non-carbonate components of this facies. The calcium carbonate content is usually above 95%. The $\delta^{13}C$ values of this facies range between 4.29‰ and 5.02‰, with an average of 4.63‰, whereas the $\delta^{18}O$ values range between –10.13‰ and –8.62‰, with an average of –9.28‰ (Tab. 1).

Interpretation

The laminated crust facies was deposited on a smooth travertine slope, fed with a constant supply of spring water. It corresponds to the smooth slope facies (Guo and Riding, 1998) or the slope facies (Shiraishi *et al*., 2020). The laminated sparite/microsparite cementstone precipitates rapidly from supersaturated parent water (Gandin and Capezzuoli, 2014; Erthal *et al*., 2017). Some traces of filamentous cyanobacteria document their presence in the sedimentary milieu; however, their role in travertine precipitation remains unclear. Unlike the laminated sparite/microsparitre cementstone, the peloids formed in the low-energy conditions of still water (Croci *et al*., 2016; Shiraishi *et al*., 2022). This suggests the occurrence of small, shallow pools on the travertine slope. The co-occurrence of different depositional sub-environments, typical of the travertine mounds, has resulted in a lateral shift of lithotypes over short distances (Guo and Riding, 1999; Claes *et al*., 2015).

The mosaic calcite, which constitutes the laminated sparite/microsparite cementstone, may have originated as a result of the diagenetic modification of a primary deposit. This lithotype is composed entirely of calcite; no traces of an aragonitic precursor were detected. Recently, only calcite travertines have been reported in Slovakia, though they are fed with highly mineralised water (Gradziński *et al*., 2015; Słowakiewicz *et al*., 2023, 2024). However, even low-magnesium calcite tufa and travertine may be affected by aggrading neomorphism, which was extensively discussed by Rainey and Jones (2007), De Boever *et al*. (2017) and Rodríguez-Berriguete (2020).

Micritic carbonate

Description

Micritic carbonate is commonly massive and structureless, though it displays indistinct layering in some parts (Fig. 5A). This facies overlies a laminated crust in logs I, II and III (Fig. 3). The boundary between these two facies is gradational. Moreover, micritic carbonate occurs over or within phytoclastic boundstone in the upper parts of logs I and IV. Imprints of grasses, twigs, tree needles and cones are visible in the facies (Fig. 5B, C). Single snail shells are found in this facies, as well. The facies is composed of two lithotypes: (i) massive microsparite cementstone and (ii) coated gas-bubble boundstone. The former lithotype predominates. It essentially consists of microsparite; however, clotted to dense micrite occurs, as well (Fig. 5D). Additionally, individual peloids are randomly distributed within this lithotype. They usually do not exceed 0.5 mm in diameter. Apart from peloids, broken, paper-thin rafts are also present (Fig. 5E). They are micrometres in thickness and arranged parallel or subparallel to the layering. The rafts are surrounded by sparite cement, display thin, micrite cores, the top and bottom surfaces of which are encrusted by sparite crystals, growing perpendicular to the cores. Fenestral pores are also common within this lithotype, and they are occasionally filled with sparite.

Coated gas-bubble boundstone was detected in log I and subordinately in log III, where it forms individual lenses, up to 30 cm in lateral dimension. The height of individual gas bubbles does not exceed a single centimetre, although they are a few millimetres in width (Fig. 5F).

The calcium carbonate content in the micritic carbonate is over 90%. The $\delta^{13}C$ values of this facies range between 3.68‰ and 4.4‰, with an average of 4.01‰, whereas the $\delta^{18}O$ values range between –8.82‰ and –8.44‰, with an average of –8.63‰ (Tab. 1).

Interpretation

Massive carbonates that may preserve imprints of flora commonly occur in a lacustrine setting (Gierlowski-Kordesch, 2010; Török *et al*., 2017). The crystallization of micrite/microsparite travertine has been linked to stagnant water, forming ponds or pools (Jones and Renaut, 2010; Özkul *et al*., 2014; Croci *et al*., 2016; Török *et al*., 2017).

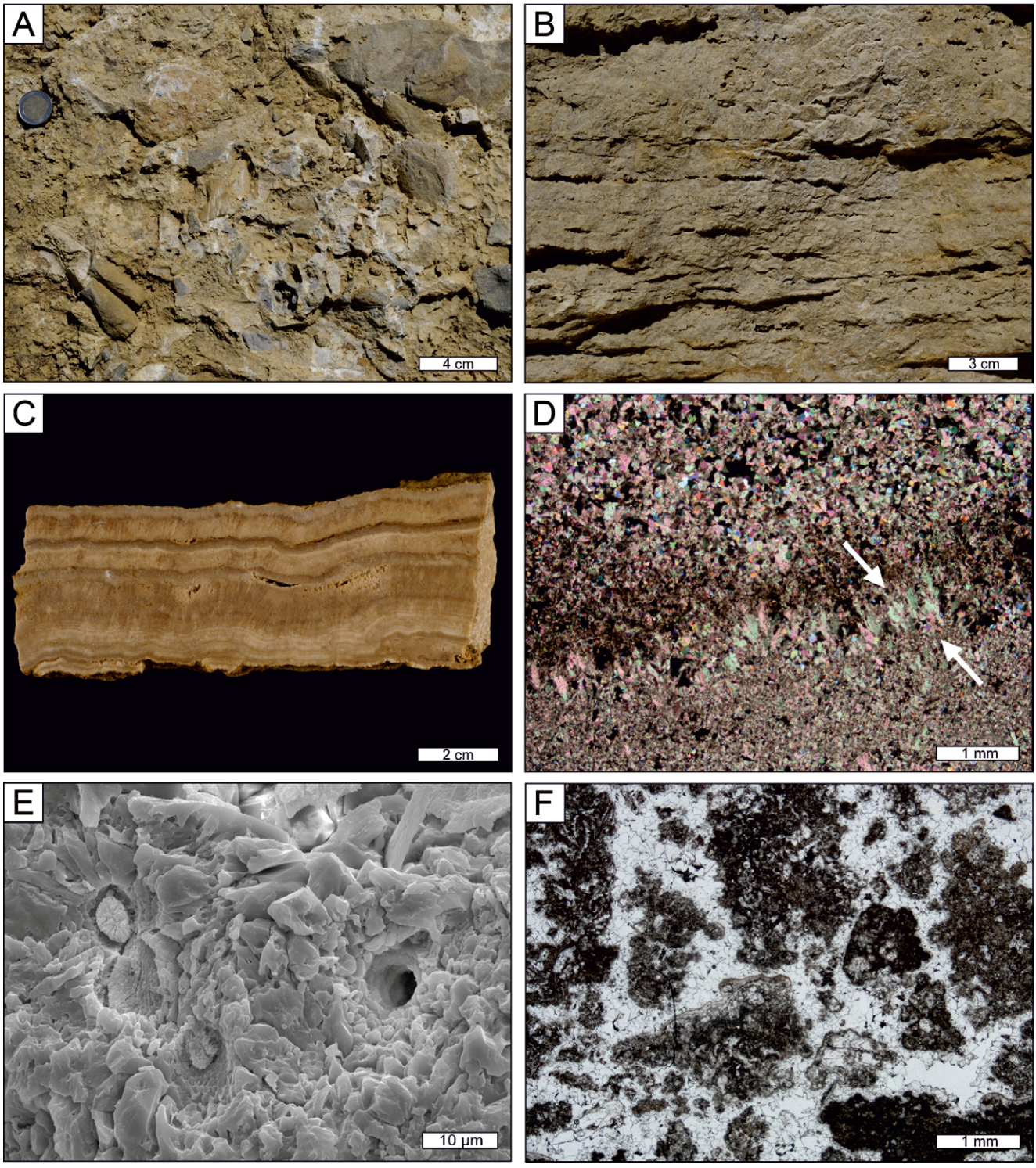

Fig. 4. Conglomerate and laminated crust. **A.** Clasts of varied sizes cemented by calcium carbonate (coin is ca. 2 cm in diameter). **B**. Laminated crust outcropping in a quarry wall. The elongated pores occur locally between consecutive beds. **C.** Polished hand sample of laminated sparite/microsparite cementstone, visible alternation of slightly undulated darker and brighter laminae. **D.** Alternation of the laminae of various micrite/microsparite contents and substituted upward by sparitic layer (microscope image, crossed-polarised light). Arrows indicate the rarely occurring feather-like crystals that grew perpendicular to the lamination. **E.** Empty moulds after cyanobacteria, encrusted by sparite (SEM-image). **F.** Peloidal grainstone, composed of aggregates of peloids of irregular shapes (microscope image, plane polarised light).

The stagnant water conditions are indicated by coated gas bubbles and paper-thin rafts, which are typical of travertines, laid down in a low-energy environment (Shiraishi *et al*., 2023). Both are also common within travertines, formed by highly mineralised water (Capezzuoli *et al*., 2014; Della Porta, 2015). Therefore, the pools, in which micritic carbonate formed were, at least partially, formed by such water. Peloids may have been formed under microbial influence (Rainey and Jones, 2009).

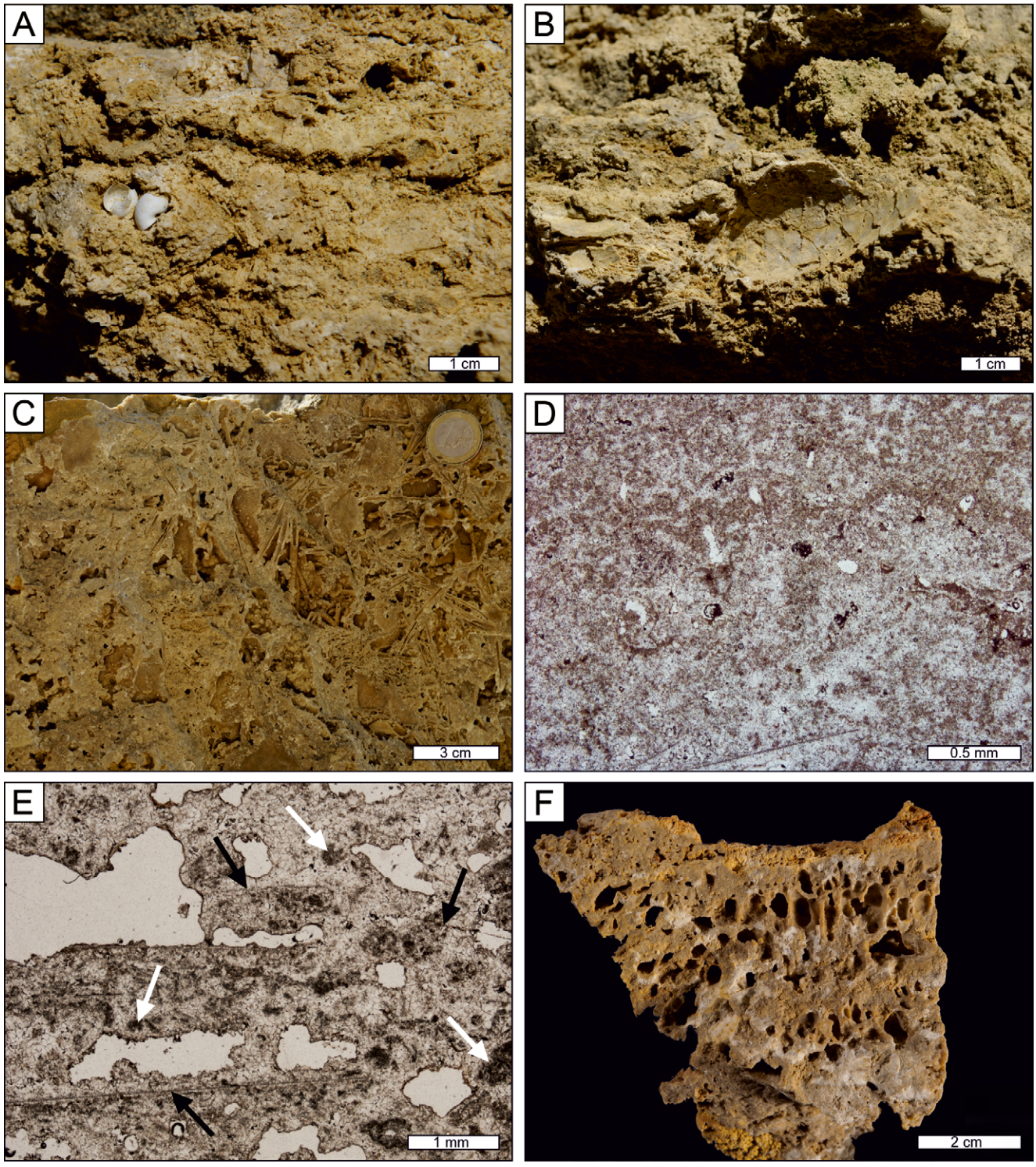

Fig. 5. Micritic carbonate. **A.** Field view; note the single snail shells. **B.** Well-preserved imprint of a cone. **C.** Moulds of the tree needles; view to the bottom of the bed (coin is ca. 2 cm in diameter). **D.** Micritic carbonate, microscope image (plane-polarised light). **E.** Fenestral porosity, peloids (white arrows) and paper-thin rafts (black arrows), (microscope image, plane-polarised light). **F.** Coated gas-bubble boundstone.

Phytoclastic boundstone

Description

Phytoclastic boundstone is the most extensive facies; it occurs in all logs studied and predominates in their upper parts (Fig. 3). The facies is distinctly layered; the layers are between 15 and 40 cm thick. The facies is dark yellow to beige in colour. Locally, the layers are orange to black, stained by manganese or iron oxides/hydroxides. A rich assemblage of malacofauna was found in the facies.

The texture and high mouldic porosity of this facies result from the presence of a huge amount of irregularly distributed phytoclasts, preserved as empty moulds (Fig. 6A, B). With a few exceptions, most of the phytoclasts are not

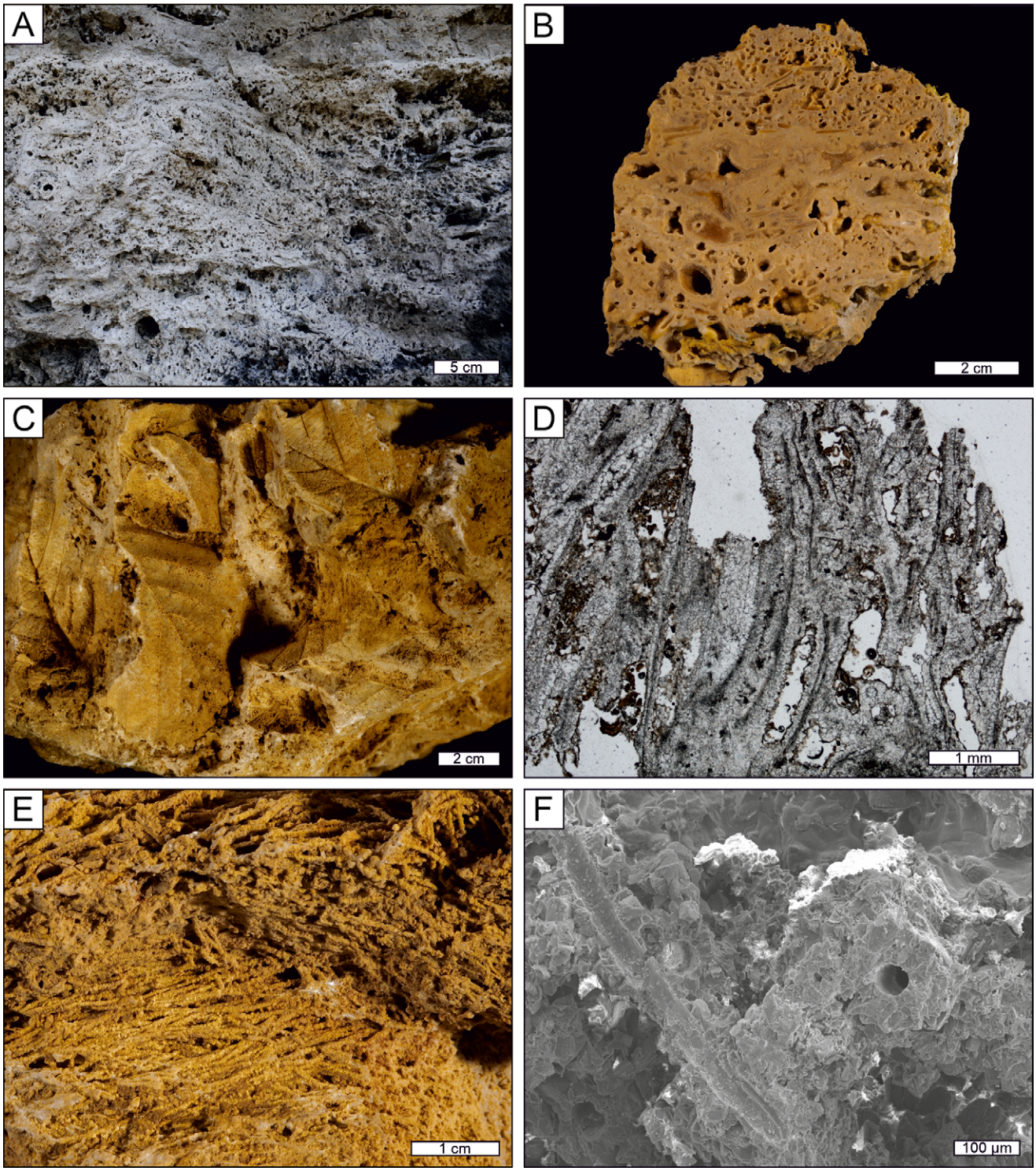

Fig. 6. Phytoclastic boundstone. **A.** Field view; note the high mouldic porosity. **B.** Polished hand sample of porous and well-cemented phytoclastic boundstone with numerous twig and tree needle encrustations. **C.** Imprints of tree leaves. **D.** Microscopic view (plane-polarised light) of calcified flora remains that form a rigid framework. Note irregularly distributed mouldic pores. **E.** Elongated algal filaments (most probably *Vaucheria* sp.). **F.** Longitudinal and transverse cross-sections of algal filaments (SEM-image).

preserved in a life position. Phytoclasts range from individual leaves and small twigs to tree logs, up to 20 cm in width (Fig. 6C). They were encrusted by calcium carbonate before decomposition of the organic matter. The encrustations create a rigid framework in this facies. They are composed of a micritic envelope, covered by sparry calcite, forming fringes up to several millimetres in thickness (Fig. 6D). Some inner parts of the empty voids after phytoclast decomposition are also partly filled with sparry calcite or detrital siliciclastics, represented mostly by the clay fraction. Ferruginous aggregates up to 2 mm in width were observed within the sparry calcite.

Phytoclastic boundstone contains abundant closely packed calcite filaments, which are visible to the naked eye

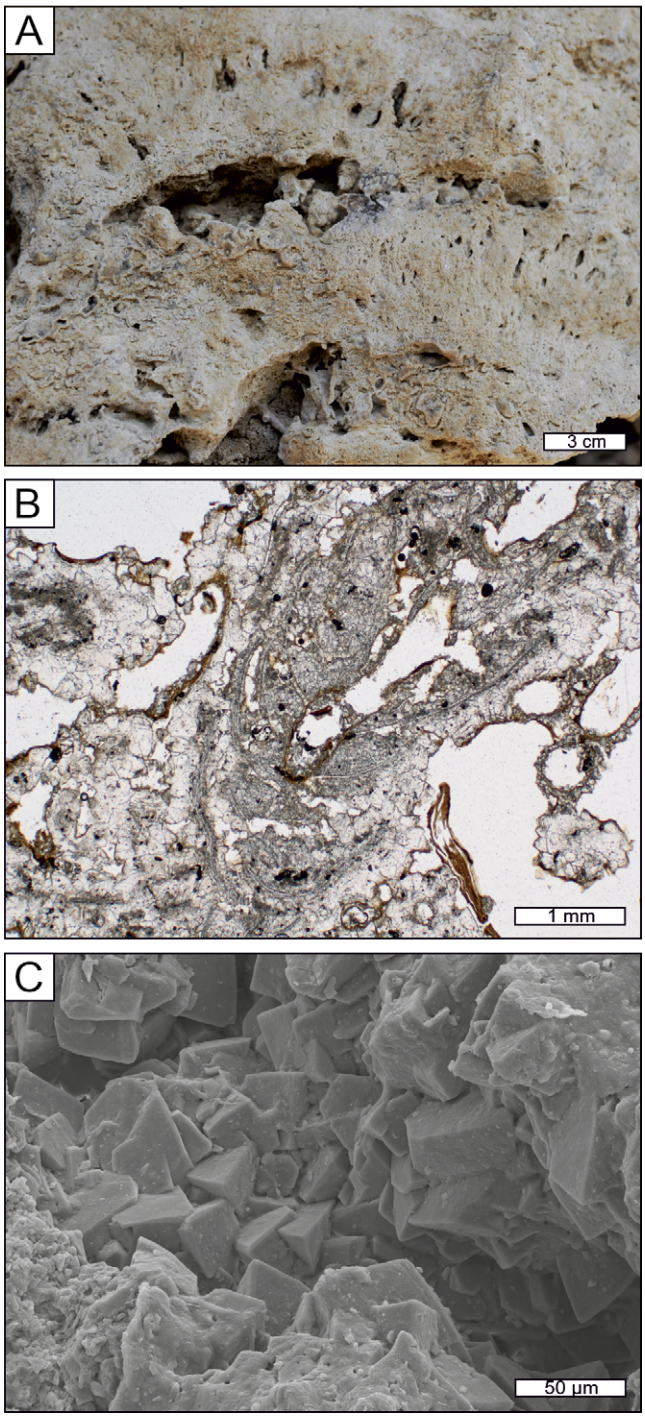

Fig. 7. Moss boundstone. **A.** Calcified moss hummock with primary porosity. **B.** Calcified moss stem with micrite-microsparite in the internal part (microscope image, plane-polarised light). Pores are partially filled by clay-size siliciclastic minerals. **C.** Sub-euhedral calcite crystals filling the pores between moss stems (SEM-image).

(Fig. 6E). The filaments are usually aligned in one direction. They are up to a dozen centimetres long and <1 mm wide. They comprise calcite crystals, which formerly encrusted algal filaments. The original algal filaments were decomposed, and their remnants are empty tubes ca. 20–30 µm in width, forming the central parts of the calcite filaments (Fig. 6F).

The measured calcium carbonate content is lower than in the other facies and ranges between 74 and >90%. The $\delta^{13}C$ values of this facies range between 3.01‰ and 5.24‰, with an average of 3.68‰, whereas the $\delta^{18}O$ values range between –9.84‰ and –8.13‰, with an average of –8.53‰ (Tab. 1).

Interpretation

The facies originated as a result of the encrustation of plant detritus, transported into the depositional environment. The category boundstone seems to be the most appropriate for the facies, since the cementation of phytoclasts took place after they had been deposited and the facies grew as a rigid framework, which resulted from the *in-situ* encrustation of porous materials, composed of plant detritus. Thus, the facies was lithified during deposition (cf. Gandin and Capezzuoli, 2014). Analogous deposits are among the most common tufa facies, especially in a riverine environment. They are documented in a plethora of papers and are referred to as phytoclast tufa (Pedley, 1990) or phytoclastic tufa (Vázquez-Urbez *et al*., 2012).

The openwork constructions built of phytoclasts were overgrown by filamentous algae. The size, spatial arrangements and dimensions of the calcified filaments suggest an affinity at least of some of them to the genus *Vaucheria*, which is commonly found in tufa-depositing streams (Pentecost, 2005; Gradziński, 2010 and references quoted therein). The parallel arrangement of filaments indicates conditions of flowing water (Freytet and Verrecchia, 1998).

A lower calcium carbonate content in phytoclastic boundstone than in the other facies documents the external input of siliciclastic material into the environment of travertine growth. Filamentous algae, constructing dense mats of overgrown phytoclastic detritus, contributed to the trapping and binding of siliciclastic grains. Microbial mats, also those composed of algal filaments, are effective binders of any supplied mineral grains (Riding, 1991; Gradziński *et al*., 2010; Suarez-Gonzalez *et al*., 2019).

Moss boundstone

Description

Moss boundstone forms lenses, up to 20 cm in width and 12 cm in height (Fig. 7A), which occur predominantly within the phytoclastic boundstone facies as individual lithosomes (Fig. 3B). The primary high framework porosity between moss stems is partly filled with sparite cement; micrite and microsparite occur subordinately (Fig. 7B, C). Some encrusted fragments of higher plants and snail shells are trapped between vertically oriented moss stems.

The calcium carbonate content of moss boundstone was between 90 and 98%. The $\delta^{13}C$ values of this facies range between 3.32‰ and 4.2‰, with an average of 3.74‰, whereas the $\delta^{18}O$ values range between –8.74‰ and –8.13‰, with an average of –8.48‰ (Tab. 1).

Interpretation

Mosses are ubiquitous in tufa depositional environments. They occur in fluvial, palustrine and perched-spring settings, present in both high-energy environment as cascades,

dams or waterfalls and low-energy ones as marshes in the poorly drained parts of fluvial valleys (Pedley, 1990; Vázquez-Urbez *et al*., 2012; Toker, 2017). Conversely, they are uncommon in the travertine depositional environment, where they are restricted to settings with relatively low temperatures (Jones and Renaut, 2010). Shiraishi *et al*. (2020) noted their occurrence in marshes, occupying the distal sites of a travertine-depositing system. The moss boundstone in the studied quarry resemble the calcified bryophyte hummocks, described by Pedley (1990) in the paludal settings of a tufa-depositing system.

Calcareous-siliciclastic mud

Description

Dark brown, calcareous-siliciclastic mud occurs within the phytoclastic boundstone only in the western part of the Čerená Quarry (logs I and II). This facies forms layers or lenses, up to a few metres in width, but only up to 2 cm in thickness (Fig. 8A). It is composed of poorly lithified, fine-grained sediments with calcium carbonate, reaching about 75% mixed with non-carbonate detritus (Fig. 8B). This includes fine-grained quartz (Fig. 8B, C), as well as muscovite, and clay minerals. The SEM-EDS investigation revealed assemblages of irregular flake-like aluminosilicate plates, which are frequently associated with calcite. The plates are usually oriented parallel to each other; their size does not exceed 5 μm (Fig. 8D). The X-ray powder diffraction of the clay-size fraction (<2 μm) points to the occurrence of kaolinite, illite, and mixed-layer illite-smectite (Fig. 8E), with a smectite content, estimated as a range of 30–40%. The $\delta^{13}C$ values of this facies range between 2.22‰ and 3.42‰, with an average of 2.92‰, whereas the $\delta^{18}O$ values range between –9.02‰ and –8.49‰, with an average of –8.74‰ (Tab. 1).

Interpretation

The accumulation of calcareous-siliciclastic mud is common in tufa-depositing systems, especially in the overbank setting of floodplains in fluvial systems (Pedley, 2009; Vázquez-Urbez *et al*., 2012; Arenas *et al*., 2014b). It denotes a stagnant or low-energy water environment of swamps or marshes. However, in travertine-depositing systems it is less common. It may indicate an efficient supply of siliciclastic material from the hinterland (Claes *et al*., 2015), During the high-water input, the fine-grained siliciclastic material could have been introduced into pools or channels, where carbonates were precipitated.

Speleothem calcite

Description

The occurrence of speleothem calcite was restricted to the uppermost part of the laminated crust in log I, where it fills a small, elongated cavity (Fig. 3B). The speleothem is up to 2 cm thick and continues horizontally for several centimetres (Fig. 9A). It is primarily composed of a columnar, elongated fabric with lateral overgrowths (*sensu* Frisia, 2015; Fig. 9B). Individual crystals are up to 4 mm long and 0.5 mm wide. The nucleation surface for calcite crystallization was formed by the peloidal grainstone lithotype of the laminated crust facies, the upper surface of which displays traces of corrosion, with pits not exceeding 0.1 mm in diameter. Similar features, but typically with larger diameters, are observed at the speleothem surface. The $\delta^{13}C$ value of the speleothem calcite is 2.77‰, whereas the $\delta^{18}O$ value is –7.63‰ (Tab. 1).

Interpretation

Columnar, elongated calcite with lateral overgrowths commonly make up speleothems (Fairchild and Baker, 2012). The discussed calcite was precipitated in a small cavity, inside the travertine formed by thermal water or by meteoric water. The relatively high $\delta^{13}C$ value supports the former possibility. However, the restricted occurrence of speleothems precludes any conclusive determination of the origin of speleothem calcite .

MALACOLOGICAL ANALYSIS

Results

The entire material included 129 identifiable specimens, belonging to 20 species, of which 13 are terrestrial species and 7 are freshwater, while 6 taxa were determined to the genus category only. Only complete or nearly complete shells extracted from travertine were registered in Table 2, but there were also a lot of less or more identifiable fragments (Fig. 5A). Most mollusc shells come from the middle part of log I (Fig. 3B). Log II contained scattered single shells only and this material was not taken into account in further considerations. Shells were found in one interval only in log IV; nonetheless, this assemblage is rather diversified.

The freshwater snails and bivalves predominate quantitatively in all of the material studied, and among them *Radix labiata* and *Anisus leucostoma* are the most numerous, particularly in intervals B and C of log I. Only in interval B a significant number of land snail species were found. In intervals A, C and D, there were single shells only, which represent the species connected to more or less open and moist habitats, such as meadows, lake shores, riverbanks, marshes and fens. They are as follows: *Vertigo antivertigo*, *Vertigo moulinsiana*, *Vallonia pulchella*, *Cochlicopa lubrica*, and a species of *Succinea*. The mollusc assemblage of interval B contains some forest and shade-loving species, preferring moist habitats: *Discus ruderatus*, *Cochlodina laminata*, *Nesovitrea hammonis*, *Fruticicola fruticum*, and *Trochulus lubomirskii*, apart from numerous freshwater *Radix labiata*. The most interesting is the typical woodland species *Discus ruderatus*, which in mountains reaches even high altitudes, as it tolerates comparatively low temperatures and is often found in post-glacial deposits.

Interpretation

The number of species and specimens in particular samples is insufficient for the estimation of a succession of mollusc assemblages and distinct environmental changes during deposition of the studied travertine. One can only state that the layers with mollusc shells from Čerená Hill

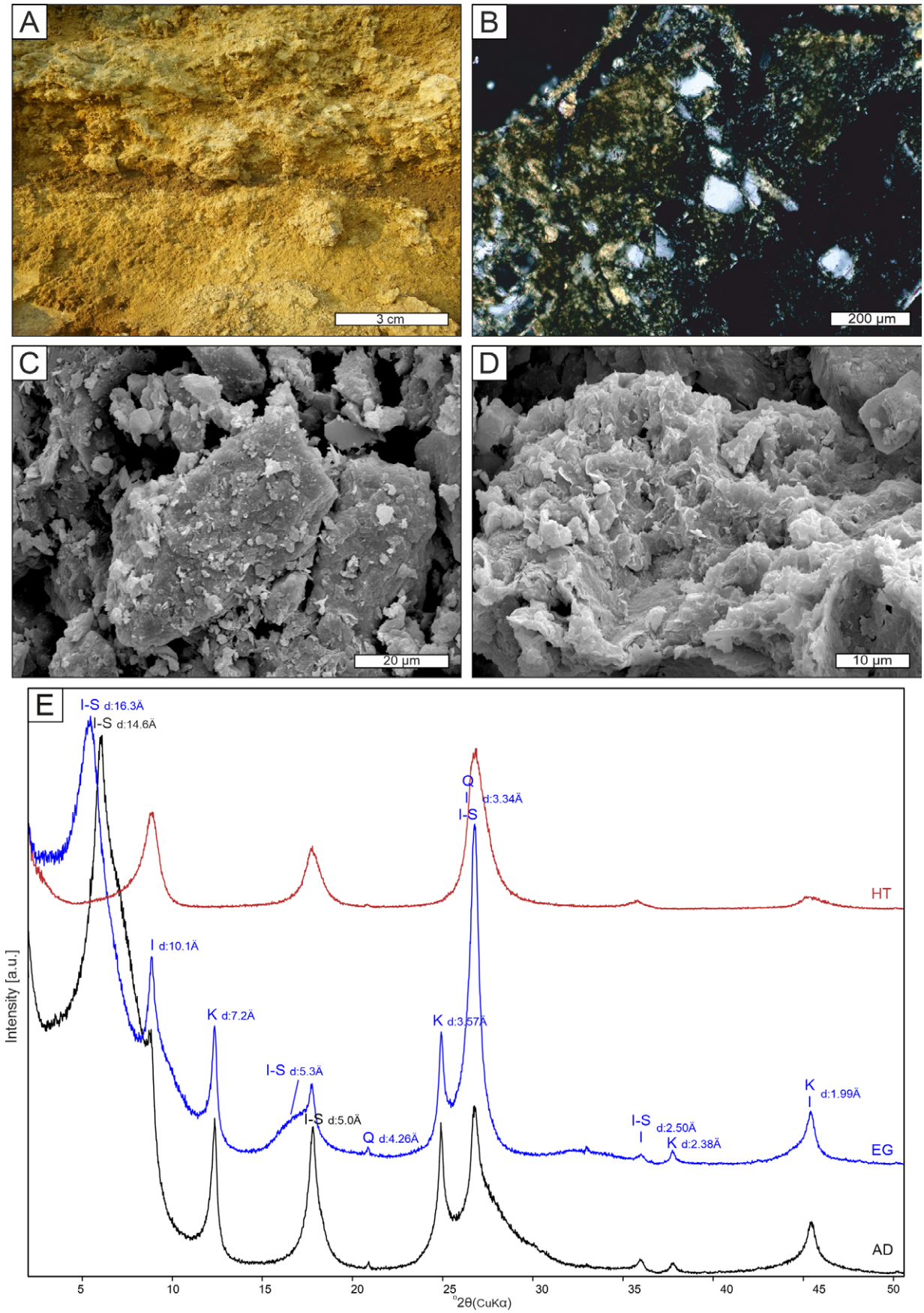

Fig. 8. Calcareous-siliciclastic mud. **A.** Brown calcareous-siliciclastic mud within phytoclastic boundstone. **B.** Singular larger quartz grains within a mixture of clay minerals and micrite (microscope image, crossed-polarised light). **C.** Quartz grains covered by clay-sized particles (SEM-image). **D.** Assemblage of shred-like scales of aluminosilicate minerals (SEM-image). **E.** Diffractogram of calcareous-siliciclastic mud. Abbreviation: I-S (illite-smectite), I (illite), K (kaolinite), Q (quartz), AD – air-dried sample, EG – ethylene-glycol-saturated sample, and HT – sample heated at 550 °C.

Table 2

Identified mollusc species.

Ecological characteristics*	Mollusc taxa	Logs and intervals					
		I				II	IV
		A	B	C	D	E	F
1	*Discus ruderatus* (Ferussac, 1821)	–	+	–	–	–	–
	Cochlodina laminata (Montagu, 1803)	–	+	–	–	–	–
	Aegopinella pura (Alder, 1830)	–	–	–	+	–	–
2	*Fruticicola fruticum* (O. F. Müller, 1774)	–	–	–	–	–	+
5	*Vallonia pulchella* (O. F. Müller, 1774)	+	+	–	+	–	+
	Vallonia costata (O. F. Müller, 1774)	–	–	–	–	–	+
7	*Cochlicopa lubrica* (O. F. Müller, 1774)	+	–	–	–	–	+
	Orcula dolium (Draparnaud, 1801)	–	–	–	–	–	+
	Nesovitrea hammonis (Strom, 1765)	–	+	+	–	–	+
	Trochulus lubomirskii (Slosarski, 1881)	–	+	–	–	–	–
9	*Oxyloma elegans* (Risso, 1862)	–	–	–	–	+	–
	Vertigo antivertigo (Draparnaud, 1801)	–	–	+	–	–	–
	Vertigo moulinsiana (Dupuy, 1849)	–	–	+	–	–	–
10	*Bithynia leachii* (Sheppard, 1823)	–	+	–	–	–	+
	Bithynia tentaculata (Linnaeus, 1758)	–	–	–	–	–	+
	Galba truncatula (O. F. Müller, 1774)	–	+	–	–	–	+
	Radix labiata (Rossmaesler, 1835)	+	+	+	–	+	+
	Anisus leucostomus (Millet, 1813)	–	+	+	–	+	+
	Pisidium amnicum (O. F. Müller, 1774)	+	+	–	–	–	–
	Pisidium casertanum (Poli, 1791)	+	–	+	–	–	+

* Ecological characteristics after Ložek (1964): 1 – typical forest species; 2 – species inhabiting mainly forest; 5 – open-country species; 7 – mesophile species of moderately humid habitats; 9 – species of very humid habitats and swamps; 10 – water molluscs.

were deposited in a humid and fairly warm climate (see also Vaškovský and Ložek, 1972; Vaškovský, 1980). However, this malacofauna does not contain significant interglacial warm species, which are characteristic for the maximum interglacial period, reported from some travertines in Slovakia (Ložek, 1961, 1973; Smolíková and Ložek, 1962).

U-SERIES DATING

Results

U-series dating results of the Čerená carbonates are presented in Table 3. The first set of samples was collected from different quarry levels. The obtained alpha-particle spectra were clear, with good energetic resolution and counting statistics. All samples, like sample CR–30, analysed using

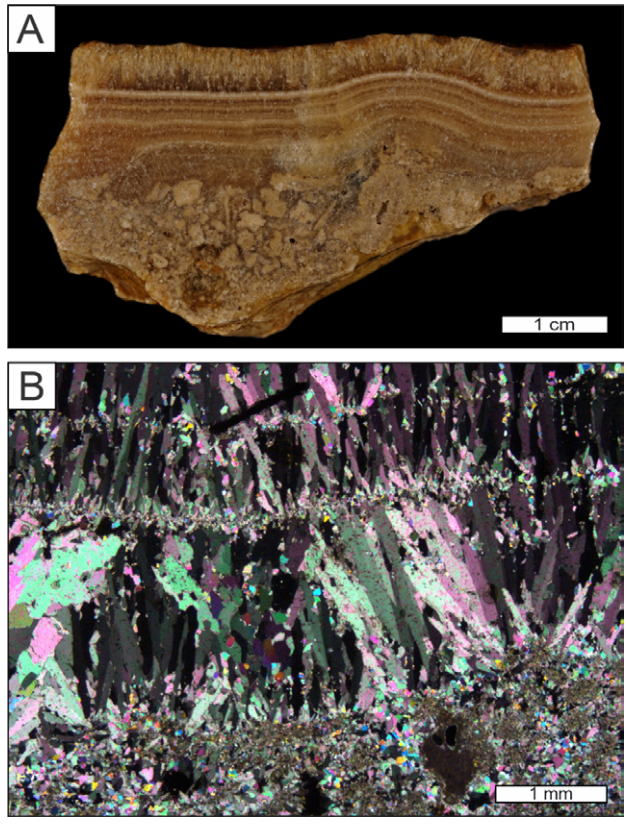

Fig. 9. Speleothem calcite. **A.** Polished sample of laminated flowstone-like speleothem covering corroded surface of peloidal grainstone (laminated crust facies). **B.** Columnar elongated fabric displaying a competitive growth pattern. The nucleation surface built by micrite peloids, cemented by sparite, in the lower part of the picture (microscope image, crossed-polarised light).

the ICP-MS method, despite careful attempts to separate clean material for analysis, contain too much non-radiogenic Th contamination, detected as the presence of ^{232}Th. Therefore, the results did not allow a reliable determination of their age without correction. Only sample CR–40 has a ^{230}Th/^{232}Th activity ratio greater than 20, allowing direct age estimation (Tab. 3). Radioactive equilibrium between ^{230}Th and ^{234}U suggests an age of the sample greater than 500 ka and the lack of equilibrium between ^{234}U and ^{238}U suggests an age below 1.2 Ma.

Interpretation

All samples had significant admixtures of allogenic thorium, indicated by low values of the ^{230}Th/^{232}Th activity ratio (below 20). Results with a high ^{232}Th content should be corrected for the initial ^{230}Th content. Generally, correction in this case refers to the subtraction of non-authigenic Th from measurement results, using ^{232}Th as an index and assuming an initial ^{230}Th/^{232}Th activity ratio in the contaminant (B0 value). A basic problem for obtaining age reliability is the estimation of the B0 value. Initial works (Kaufman and Brocker, 1965; Kaufman, 1993; Lin *et al*., 1996), based on analyses of detritus obtained from carbonate samples, suggested using a ^{230}Th/^{232}Th activity ratio of 1.7 ± 0.7. On the basis of these works, values of 1.5–1.7 are used as a correction factor (Schwarcz, 1980; Onac *et al*., 2002; Constantin *et al*., 2007; Linge *et al*., 2009). Different values of the ^{230}Th/^{232}Th activity ratio usually are used without detailed discussion (e.g., Fleitmann *et al*., 2004, used a value of 3.8). In some papers, the authors use information from the detritus extracted from carbonates (Dorale *et al*., 1992; Dykoski *et al*., 2005). Others use a value of 0.84 ± 0.42, reflecting the average composition of the continental crust (Baker *et al*., 1996; Xia *et al*., 2001; Wang *et al*., 2001; Zhao *et al*., 2003; Cruz *et al.*, 2005; Li *et al*., 2005; Cosford

Table 3

Results of alpha spectrometry and ICP-MS dating of Čerená spring-related carbonates.

Sample	Lab. No.	U [ppm]	^{234}U/^{238}U	^{230}Th/^{234}U	^{230}Th/^{232}Th	Age [ka]	*B0	Corrected Age [ka]
Alpha spectrometry								
CR–1A	W 3134	0.26 ± 0.02	1.21 ± 0.06	1.01 ± 0.04	17	+ 84 340 - 52	1.5 ± 0.5	+ 89 330 - 60
							0.84 ±0.42	+ 67 330 - 47
CR–1B	W 3131	0.32 ± 0.02	1.18 ± 0.04	0.97 ± 0.04	17	+ 38 385 - 30	1.5 ± 0.5	+ 45 280 - 37
							0.84 ± 0.5	+ 50 280 - 38
CR–2	W 3150	0.31 ± 0.02	1.30 ± 0.05	1.06 ± 0.04	15	+ 130 420 - 66	1.5 ± 0.5	+ 137 410 - 74
							0.84 ± 0.42	+ 166 408 - 76
CR–4	W 3133	0.30 ± 0.02	1.23 ± 0.05	1.06 ± 0.04	11	+ inf. 480 -100	1.5 ± 0.5	+ inf. 470 -112
							0.84 ± 0.42	+ inf. 478 - 113
ICP-MS								
CR–40	400	0.3321 ± 0.0006	1.178 ± 0.003	1.089 ± 0.006	22.7 ± 0.1	> 500 < 1.2 Ma		
CR–30	401	0.2575 ± 0.0005	1.178 ± 0.004	0.883 ± 0.006	10.26 ± 0.06	208 ± 4	1.5 ± 0.5	194 ± 12
							0.84 ± 0.42	201 ± 11

*B0 – assumed initial ^{230}Th/^{232}Th activity ratio in contaminant.

et al., 2008; Lundberg *et al*., 2010). They arbitrarily assume an error at the level of 50%.

The present authors decided to check two B0 values for age estimation of the Čerená carbonates. The first one (1.5 ± 0.5) covers the main published $^{230}Th/^{232}Th$ activity ratio range. The second one (0.84 ± 0.42) refers to the average composition of continental crust. The results of both correction methods agree in the error range. There are no big differences between corrected and uncorrected ages, as might be expected for old samples with a relatively high uranium content.

PALAEOMAGNETIC AND PETROMAGNETIC ANALYSIS

Results

The palaeomagnetic properties of oriented laboratory samples (a total of 83 analyses) were investigated. They are characterised by a large scatter, both of the NRM intensity (0.06–3.91 mA · m^{-1}, average 0.60 mA · m^{-1}, standard deviation 0.55) and the MS values (–10.8 to 36.3 × 10^{-6} SI units, average 2.02 × 10^{-6} SI, standard deviation 12.01).

Each of the studied samples was subjected to TD or AF demagnetisation in 12–14 temperatures or fields. The samples yielded reliable palaeomagnetic directions. The A-components of remanence are mostly of viscous or chemo-remanent (weathering) origin; they can be removed by AF demagnetisation with an intensity of 5–10 mT and/or by TD at temperatures of 80–120 °C. The ChRM (high-field) component is stable and can be isolated in the AF (ca. 15–80 mT) and/or in the temperature range of 160–520 °C.

Except for thirteen samples with very low intensity, the maximum angular deviation (MAD) values are generally lower than 10°; therefore, the palaeomagnetic directions are well determined. Samples with MAD values greater than 10° are interpreted with transient polarity. The ChRM directions were clearly dominated by normal (N) polarity (positive inclinations) and/or reverse (R) polarity (negative inclinations). To test the possible influence of phase changes of magnetic minerals during laboratory TD processing, diagrams of *kt*/*kn* values *vs* laboratory thermal demagnetising field t (°C) were also constructed for the samples.

The results of TD and AF demagnetisation procedures are displayed in Figure 10. It refers to two samples with N palaeomagnetic directions (Fig. 10A–B) and two samples with R palaeomagnetic directions (Fig. 10C–D). Analogous results were obtained for most samples through the section.

Rock magnetic properties throughout the section show magnetite (blocking temperature T: 520–560 °C) as the main magnetic fraction. The results of the IRM measurements, demonstrated on two samples in Figure 11, show that some of the magnetic particles display low magnetic hardness. The IRM acquisition showed that all samples reached magnetic saturation by 120 to 200 mT. Backfield demagnetisation of the saturation IRM revealed a coercivity of remanence between 20 to 40 mT in general.

The mean directions and dispersions of components were calculated, using Fisher's statistics (Fisher, 1953), and were displayed on a Wulf stereographic projection. They are marked either by full or empty crossed circles, with a confidence circle, circumscribed around the mean direction at the 95% probability level (Fig. 12). Both magnetic polarities are present in the ChRM component directions (Tab. 4).

The resulting magnetostratigraphic profile is shown in Fig. 13. Individual magnetozones are clearly manifested in a discriminant function defining the polarity (Man, 2008). The values of the mean palaeomagnetic declination and inclination (Tab. 4) in the group with R polarity show a higher variance than the N polarity group (α_{95} values). Higher scattering results from a small number of samples (6), with R polarity in the upper part of the studied profile.

Interpretation

N and R magnetic polarities were interpreted on the palaeomagnetic profile (Fig. 13). The values of palaeomagnetic directions, especially the declinations, show a considerable variation and a significant difference between the upper and lower parts of the profile. The mean value of the palaeomagnetic declination (17.1°), calculated without anomalous samples with N? polarity, represents a value different from the current declination (2°). In the upper section of the profile, a narrow zone with R polarity was found but also with a significant anomalous value of the palaeomagnetic declination (157°, Tab. 4), which would probably be correlated with the geomagnetic field excursion. Owing to U-series dates, which are reliable only at the top of log IV (ca. 208 ka), the excursion of the magnetic field could represent Jamaica-Pringle Falls (ca. 211 ka; Singer, 2014) or some of the younger excursions.

Table 4

Mean palaeomagnetic directions. Note: N – normal polarity; R – reverse polarity; D, I – declination and inclination of the remanent magnetisation; α_{95} – semi-vertical angle of the cone of confidence, calculated according to Fischer (1953) at the 95% probability level; k – precision parameter; n – number of samples.

Locality	Polarity	Mean palaeomagnetic directions		α_{95}	k	n
		D	I			
		[°]				
Čerená	N	17.1	67.89	2.79	41.49	64
	R	157.29	-73.84	4.76	144.25	6

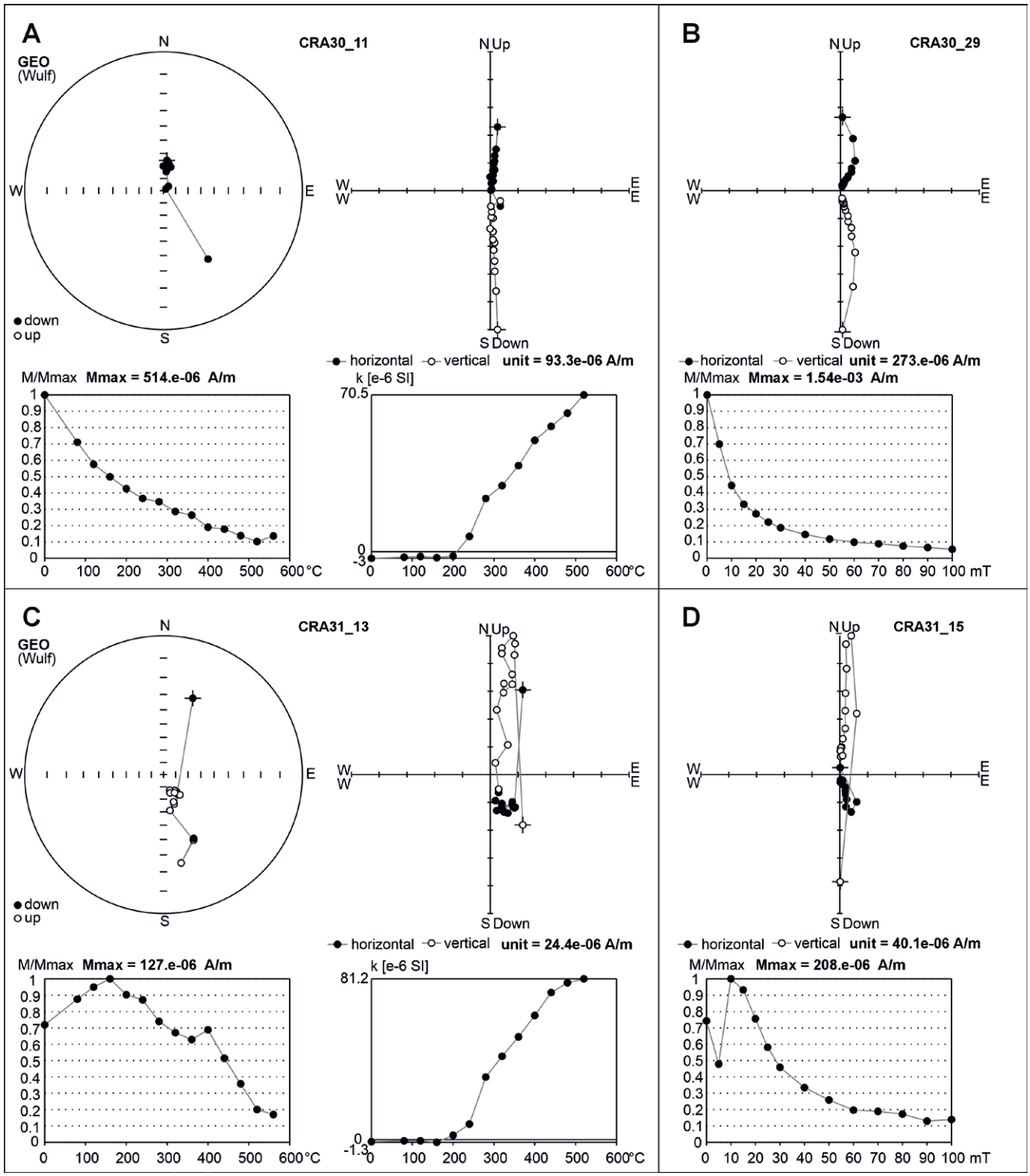

Fig. 10. Results of sample demagnetisation with N (A–B) and R (C–D) palaeomagnetic polarity. **A.** Thermal demagnetisation of the CR30 sample. **B.** Alternating field demagnetisation of the CR30 sample. Upper left: A stereographic projection of the natural remanent magnetisation of a sample in the natural state. Upper centre and right: Zijderveld diagram – full circles represent projection on the horizontal plane (XY), empty circles represent projections on the north–south vertical plane (XZ). Lower left and lower right: graph of normalized values of the remanent magnetic moments versus thermal (A) and/or alternating (B) demagnetising fields; M – modulus of the remanent magnetic moment of a sample, subjected to thermal demagnetisation. Lower centre: graph of the normalized values of volume magnetic susceptibility versus thermal demagnetising fields; k – value of volume magnetic susceptibility of a sample, subjected to thermal demagnetisation (A). **C.** Thermal demagnetisation of the CR31 sample. **D.** Alternating field demagnetisation of the CR31 sample. Description the same as in A–B.

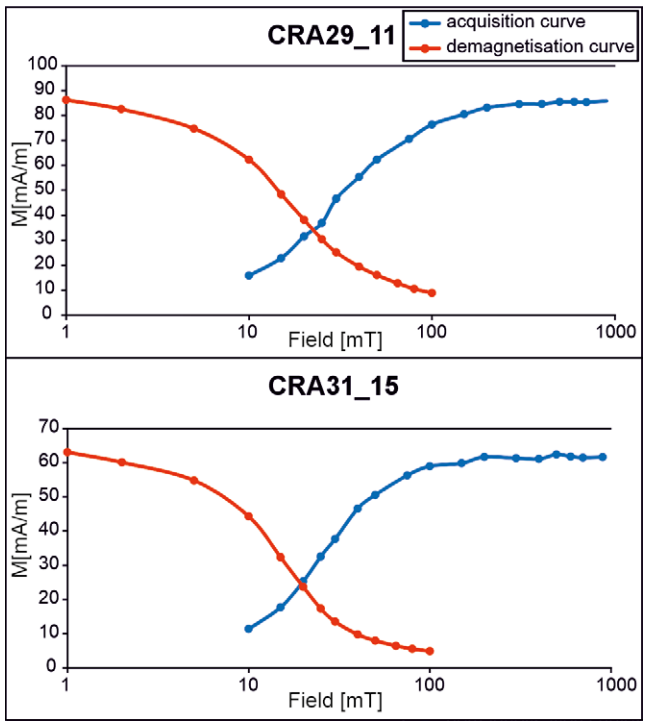

Fig. 11. Examples of isothermal remanent magnetisation acquisition and alternating field demagnetisation curves.

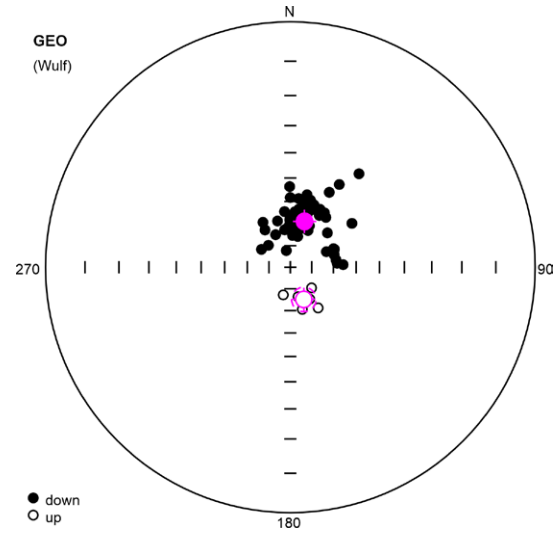

Fig. 12. Mean directions of the characteristic remanent magnetisation components with normal (full) and reverse (open) palaeomagnetic polarity. Stereographic projection, full (open) small circles represent projection onto the lower (upper) hemisphere. The mean directions, calculated according to Fisher (1953), are marked by a small pink cross across a circle; the confidence circle at the 95% probability level is circumscribed about the mean direction.

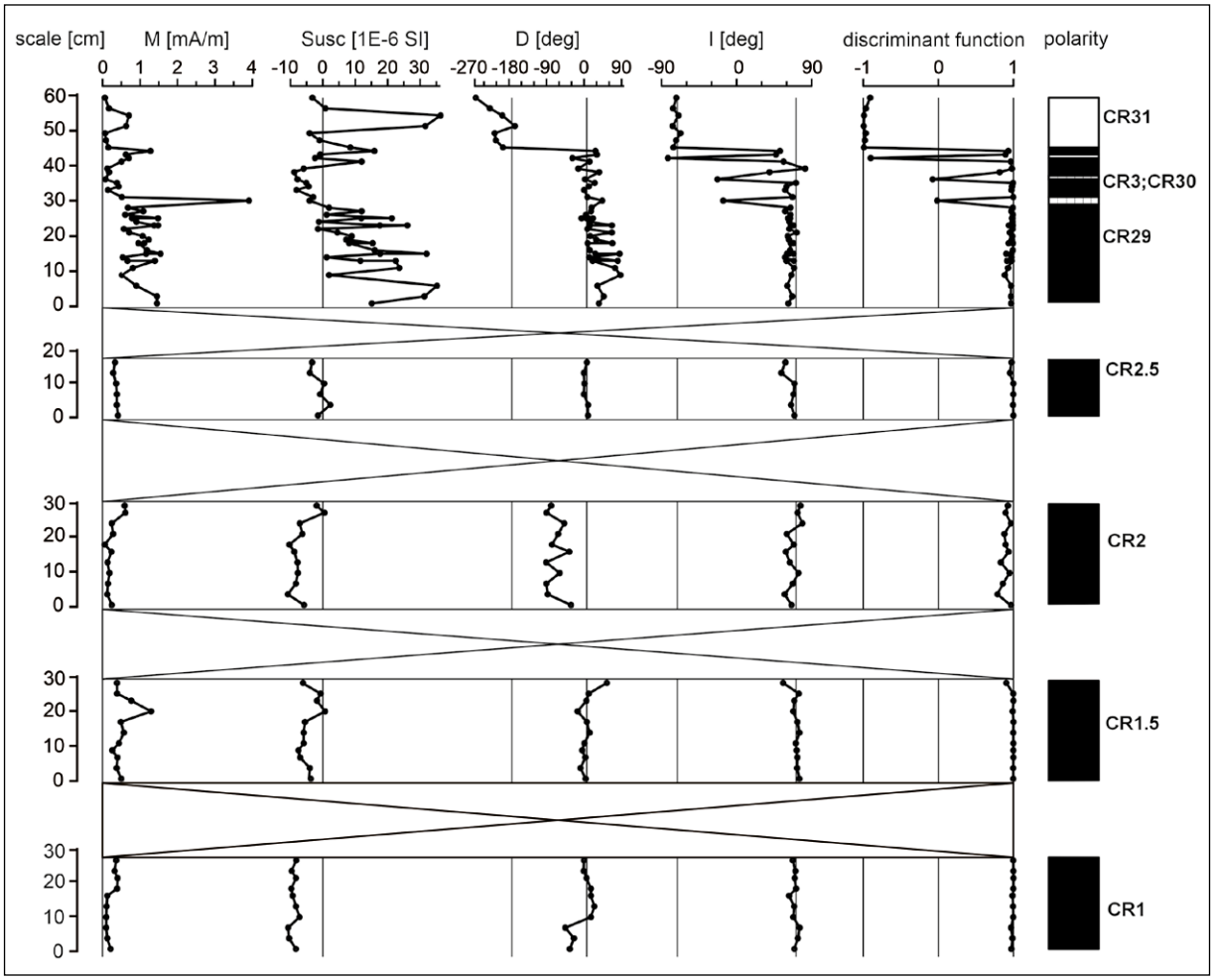

Fig. 13. Basic magnetic and palaeomagnetic properties. Black – normal polarity, white – reverse polarity, shaded – transitional polarity, M – the modulus of the natural remanent magnetisation, Susc – magnetic susceptibility of samples in natural state, D – declination, I – inclination, and a discriminant function defining the polarity. Position of samples indicated in Figure 3.

DISCUSSION

Parent fluid

An indirect indicator of the parent fluid origin may be the carbon stable isotope ratio of the studied travertine. Typical travertines fed by deep circulation water are characterised by high $\delta^{13}C$ values (generally over –1‰; Pentecost, 2005, p. 143). The $\delta^{13}C$ values of the studied travertines range between 2.22‰ and 5.24‰, with an average of 3.68‰ (Fig. 14A), that is over this conventional threshold boundary. This suggests that the travertines were fed by ascending water, highly charged with CO_2 of deep origin (e.g., Crossey *et al*., 2006). The isotopically heavy CO_2 may have originated from metamorphic decarboxylation of carbonate rocks or from magmatic sources.

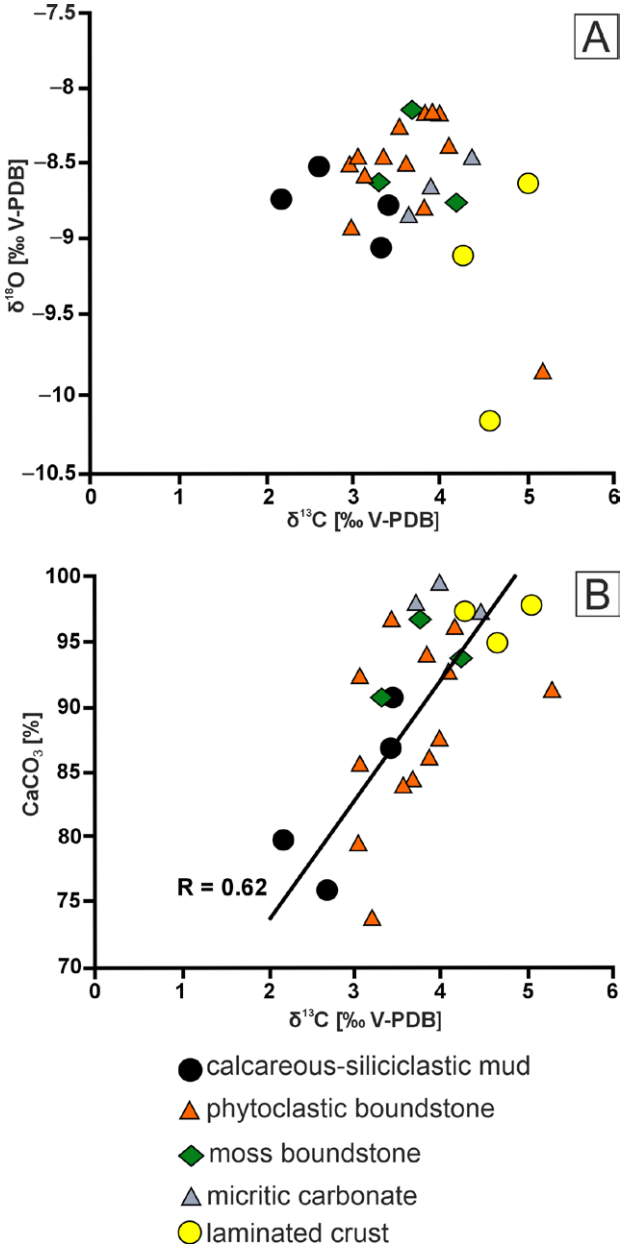

Fig. 14. Carbon and oxygen stable isotope composition of spring-related carbonates. **A.** Carbon and oxygen stable isotope composition of particular facies. **B.** Correlation of calcium carbonate content and $\delta^{13}C$ values; correlation coefficient r = 0.62.

Crystallising calcium carbonate typically has higher $\delta^{13}C$ values than the parent CO_2 (e.g., Hoefs, 2018). To describe this relationship, the following empirical equation, developed for Italian travertines by Panichi and Tongiorgi (1976), is used:

$$\delta^{13}C_{gas.} = 1.2\ \delta^{13}C_{trav.} - 10.5.$$

This equation provides only approximate values, as the isotopic signal of travertines depends on many additional factors that interact during crystallisation (e.g., Chafetz *et al*., 1991; Liu *et al*., 2003; Kele *et al*., 2008, 2011). Despite this, it has recently been used to estimate $\delta^{13}C$ of CO_2 in solutions, feeding fossil travertines (e.g., Claes *et al*., 2017; Török *et al*., 2017, 2019). In the case of the studied travertines, the application of the above equation suggests that the $\delta^{13}C$ of CO_2 in the parent fluid ranged from –7.5‰ to –4.5‰. These values are similar or slightly lower than the currently measured $\delta^{13}C$ of CO_2 in deep circulating water in the Western Carpathians. Cornides and Kecskés (1982) report values between –2.4‰ and 5.1‰ for neighbouring sites in the Liptov Basin, while Povinec *et al*. (2010) report a value of –6.5‰.

Slightly lower values may suggest the isotopic modification of CO_2 during upflow to the surface in the shallow zone of the aquifer (Leśniak, 1998) or mixing with biogenic CO_2, originating from soil production and present in shallow circulation waters. Such mixing may also occur in the shallow zone of the aquifer (Brogi *et al*., 2012; Mohammadi *et al*., 2020; Gori *et al*., 2024). In the case in question, however, it most likely already occurred on the surface during contact between deep circulation waters and surface waters with biogenic CO_2. This scenario is indicated by: (i) the distribution of $\delta^{13}C$ values for individual facies, where the highest values characterise facies typical of travertines, i.e., crystalline crusts and micritic travertine, and (ii) the inverse correlation between $\delta^{13}C$ and calcium carbonate content (Fig. 14B). The latter relationship implies that non-carbonate components were supplied by waters, containing isotopically light CO_2 (i.e., surface runoff waters). However, it should be emphasised that the generally high $\delta^{13}C$ values of CO_2 in the parent solution testify to the precipitation of the studied travertines from a solution, dominated by isotopically heavy CO_2 of deep origin (e.g., Crossey *et al*., 2006; Pentecost, 2005). It can therefore be assumed that this was analogous to the CO_2, emanating today in many parts of the Western Carpathians, which originates from the thermal decomposition of Mesozoic carbonates (Leśniak, 1998; Povinec *et al*., 2010, see also review in Kucharič *et al*., 2015). Several springs, expelling water highly charged with CO_2 of deep origin, occur in the Liptov Basin; some of them are located in the vicinity of the studied carbonate complex.

Depositional setting

The studied carbonate complex was formed in a mid-mountain basin, bordered by faults. The spatial relationship of travertines and the faults, which acted as conduits delivering highly mineralised deep circulation water to the surface, is typical of travertines all over the world (e.g., Hancock *et al*., 1999; Brogi *et al*., 2010, 2014, 2018; Priewisch *et al*.,

2014; Van Noten *et al*., 2019; Mancini *et al*., 2021). The immediate substrate of the studied travertines is an alluvial-fan sediment. The association of travertines and sediments of alluvial or colluvial fans is common in fault-bounded basins (e.g., Croci *et al*., 2016; Scalera *et al*., 2022; Varejão *et al*., 2025). This association results from the genetic relationship between travertines and alluvial or colluvial fans with active faulting. Furthermore, the geochemical characteristics of the studied deposits strongly suggest their genetic affinity to deeply circulating fluids (see above section, 'Parent fluid').

The springs supplied water of the deep circulation to the marshy floodplain, situated at the foot of the Low Tatra Mts, which acted as a recharge area (Figs 15, 16). The location of the source springs, which were the input point of highly mineralised water into the carbonate depositional system, is unknown. It most probably was dependent upon the course of the fault, cutting the impermeable Palaeogene bedrock. The fault guided water, charged with CO_2 of deep origin, which ascended to the surface, as is the case today in many places in the Central Western Carpathians (Cornides and Kecskés, 1982; Franko and Šivo, 1999; Franko, 2001; Povinec *et al*., 2010). The outflows most probably had a point character, since the over-pressured water migrated to the surface through uncemented or poorly cemented conglomerates of an alluvial fan (see Hancock *et al*., 1999; Brogi and Capezzuoli, 2009; Capezzuoli *et al*., 2014).

The marshy area was a mosaic of sub-environments, which determined today's mosaic arrangement of facies (Fig. 15). Near the spring orifice, laminated crusts formed, probably building small spring mounds, surrounded by submerged areas, where micritic carbonate facies formed. Some parts of this area were also within the range of streams, flowing from the south from the Low Tatra Mts (Fig. 16A). These parts were fed with diluted water, which was a mixture of the deep-circulation component and surface stream water. Phytoclastic boundstone facies and isolated hummocks, built of moss boundstone, were formed there. Individual layers of siliciclastic calcareous mud are a record of high-discharge episodes. They can represent the overbank flow deposits of fluvial systems (Della Porta *et al*., 2017; Scalera *et al*., 2022) or alluvial fans (Brierley *et al*., 1991) and can be deposited from suspension or as mudflow deposits (Zieliński, 2014). The dominance of the phytoclastic boundstone facies in the upper part of the complex and the occurrence of laminated crusts only in its lower part suggest a greater influence of surface waters over time (Figs 3, 15). This may be related to the decline in the activity of the spring or the lateral migration of facies. The size of the studied outcrop makes it impossible to resolve this issue.

The studied complex of spring-related carbonates was laid down out of reach of the main fluvial channels, which is evidenced by the absence of gravel intercalations within

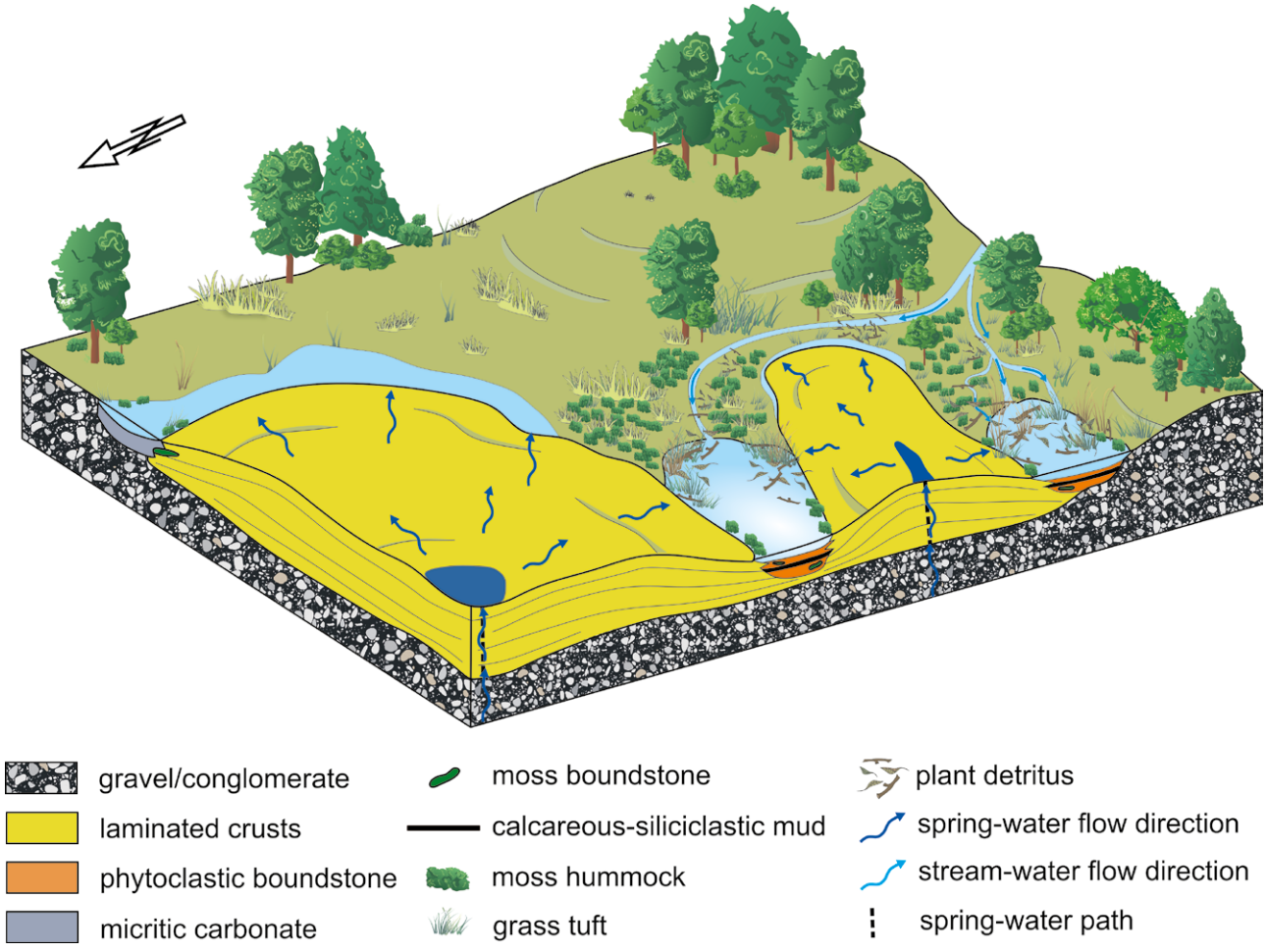

Fig. 15. Depositional environment of the hybrid spring-related carbonates, schematic model.

the carbonates. This view is further supported by the lack of syndepositional erosion traces, which could be genetically related to the incision of fluvial channels during high-discharge events (see Luo *et al*., 2021). In turn, the occurrence of fine-grained siliciclastics proves that flooding water could have spread over the depositional environment of the studied carbonates. Therefore, the absence of gravel and the presence of fine-grained siliciclastic material collectively indicate deposition of the carbonates studied in the unconfined setting of a floodplain. However, the studied deposits differ from the travertines, deposited in an unconfined setting at the foot of the mountains, being in the reach of alluvial or colluvial fans. Such situations were described by Wang *et al*. (2016) from Tibet as well as by Aguillar *et al*. (2024) and Varejão *et al*. (2025) from the Andean Altiplano in Argentina. In the first case, Pleistocene and Holocene travertines were repeatedly covered by cohesive debris-flow sediments of colluvial origin. In the second case, travertines were invaded by ephemeral rivers that deposited interlayered siliciclastic sediments, including conglomerate and sandstone. Therefore, the described spring-related carbonates were formed at a distance from active alluvial or colluvial fans, having been developed at the toe of the Low Tatra Mts slopes.

Facies contrasts: are the deposits studied more calcareous tufa or travertine?

A characteristic feature of the hybrid spring-related carbonates is the contrast of the facies. This is manifested in the lateral juxtaposition and vertical succession of facies, typical of travertines and calcareous tufas. The former include laminated crusts and micritic travertine, whereas the latter include phytoclastic boundstone and moss boundstone (Fig. 3). The discussed carbonate complex is also characterised by the common occurrence of molluscs and intercalations of calcareous mud, which are typical of tufa, but not of travertine. This proves that the rock series under study was formed in a specific setting, intermediate between travertine and tufa depositional environments.

The phenomenon of lateral gradational transition from typical travertines in spring settings to sediments with tufa-like fabrics in more distal settings is common in travertine depositional environments. This is the result of a decrease in temperature and the mineralisation of water with increasing distance from the feeding spring. This creates conditions for colonisation by algae and higher plants, resulting in sediments with numerous encrusted plants. A typical example is the reed travertine lithotype, defined by Guo and Riding (1998), which is commonly found in the distal parts of travertine systems.

The sediments described to some extent appear to correspond to travitufa (*sensu* Capezzuoli *et al*., 2014), but their formation was more complex and cannot be explained solely by changes in temperature and water chemistry along the flow out of the spring orifice. In the distal part of many travertine systems, higher plants are often found, but they are mainly preserved in their original growth position (e.g., Guo and Riding, 1998; Özkul *et al*., 2013; Capezzuoli *et al*., 2014; Claes *et al*., 2015, 2017; Toker *et al*., 2015; Mors *et al*., 2019; Janssens *et al*., 2020; Mohammadi *et al*., 2020). On the other hand, the common presence of phytoclastic boundstone facies in the studied travertines indicates the deposition of plant detritus, including tree trunks, and its subsequent encrustation with calcium carbonate. This process is typical of a tufa depositional environment (e.g., Pedley, 1990; Vázquez-Urbez *et al*., 2012; Gradziński *et al*., 2013; Arenas *et al*., 2014b; García-García *et al*., 2014). It indicates the presence of a flow that transported plant detritus and thus testifies to the occurrence of a plant community in the catchment (Figs 5, 6). Similar processes have been observed in environments, where deep circulation water mixes with surface stream water (Toker, 2017; Tagliasacchi and Kayseri-Özer, 2020; Luo *et al*., 2021). The latter is responsible for transporting plant detritus to the depositional milieu. Luo *et al*. (2021) proposed the term phytoclast rudstone for such facies of fluvial travertine. Phytoclastic rudstone/packstone, identified by Croci *et al*. (2016) in Miocene travertine, can serve as another possible analogue. Along with plant detritus, the shells of terrestrial molluscs were also transported. They are present notably in interval A of log I, composed of phytoclastic boundstone with calcareous-siliciclastic mud intercalations (Fig. 3). The occurrence of terrestrial molluscs was also stressed by Vaškovský and Ložek (1972) and Vaškovský (1980).

What distinguishes the studied deposits from calcareous tufas and from fluvial travertines is the above-mentioned absence of incorporated gravel. It commonly occurs in calcareous tufas (Vázquez-Urbez *et al*., 2012) as well as in fluvial travertines, formed in the confined settings of narrow and deeply incised valleys, as is the case in Ngol, Cameroon (Bisse *et al*., 2018), Bagni San Filippo, Tuscany, Italy (Luo *et al*., 2021) and Las Temises, Gran Canaria, Spain (Rodríguez-Berriguete *et al*., 2022).

Age of the studied complex

The U-series dating results obtained are affected by a large uncertainty (Tab. 3). Data from the top of the complex indicates an age of 208 ka, which corresponds to MIS7a. This age defines the end of sedimentation of the studied complex. However, it is not possible to determine when sedimentation began. It can only be assumed that it was around 330 ka. This is consistent with the results of palaeomagnetic analysis (Figs 10, 13). Normal polarity, with the exception of that associated with some reverse polarity excursion (presumably the Jamaica-Pringle Falls excursion), indicates that the entire complex was formed during the Brunhes Chron, i.e., in the last 773 ka. The deposition of spring-related carbonates was preceded by the partial cementation of the underlying alluvial-fan conglomerate. The sparry cement, dated at between 0.5 and 1.2 Ma, indicates an upper time limit of conglomerate deposition (Tab. 3, sample CR-40); however, the precise time remains unknown.

The growth rate of spring-related carbonates is estimated at millimetres per year for tufa, but at centimetres per year for travertine (see discussion in Gradziński, 2010). Taking this into account, as well as the thickness of the studied deposits, it can be assumed with a high probability that

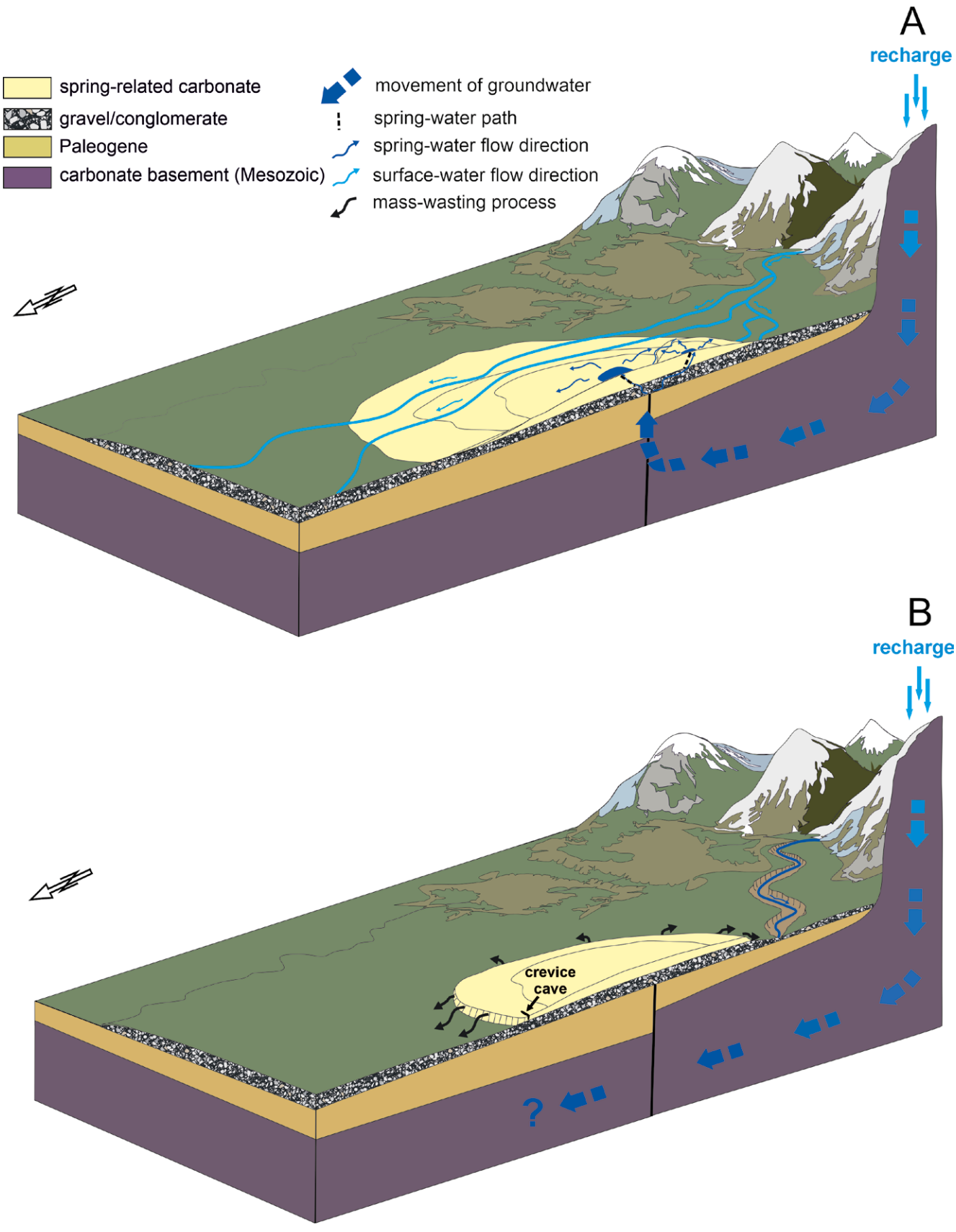

Fig. 16. General conceptual model, illustrating the evolution of Čerená Hill. **A.** Deposition of the spring-related carbonates at the foot of the mountains within the marshy floodplain, fed with a mixture of deep-circulating water, issued by spring and surface runoff . **B.** Incision of the valleys, cessation of spring activity and shaping of the hill by mass-wasting processes.

the studied complex contains hiatuses, which are records of breaks in its growth. They have not been identified, due to the current state of exposure of the complex. It seems likely that the hiatus is located in the segment between 3.5 m and 5 m of log IV (Fig. 3), which is inaccessible, due to being covered by rubble.

Palaeoenvironmental significance

Although travertine deposition is independent of biogenic carbon dioxide of soil origin, it is indirectly dependent on climatic conditions. An important factor is the supply of water from aquifers to the surface, which in turn requires the aquifers to be fed by precipitation. Dating of Pleistocene travertines has shown that many of them grew during periods of warm and humid climate (Rihs *et al*., 2000; Faccenna *et al*., 2008; De Filippis *et al*., 2013; Mancini *et al*., 2021; Brilli and Giustini, 2023). However, this relationship is not very precise, which is due to the time delay, resulting from the residence time of deep circulation water in an aquifer; this can up to tens of thousands of years. The residence time of contemporary waters in the Central Western Carpathians is estimated to be from 8.7 ka to over 30 ka (Franko and Šivo, 1999; Franko, 2001). In the case of the studied fossil travertines, the residence time of the feeding water is unknown. Despite this uncertainty, it can be hypothesised that the deposition of the studied travertines was related to the conditions of the Pleistocene warm-climatic phases. This is also evidenced by the presence of plant detritus, including leaves, tree needles, cones, and tree trunks, which can be collectively regarded as an indicator of mixed forest occurrence in the catchment (Figs 5, 6). This notion is partly supported by the obtained mollusc data, despite some of their indistinctness (Tab. 2), as well as the previous results, obtained by Vaškovský and Ložek (1972).

Unfortunately, the wide-error dating of the travertines studied makes it impossible to pinpoint when such conditions occurred (Tab. 3). The top part of the carbonate is dated at ca. 208 ka, which corresponds to MIS7a. At that time, the crystallisation of speleothems was recorded in the nearby Demänová Cave System (Bella *et al*., 2021; Błaszczyk and Hercman, 2022) and in the caves of the Tatra Mts (Błaszczyk *et al*., 2020). Simultaneously, spring-fed travertines were formed at Vyšné Ružbachy (Vieira *et al*., 2023). The bottom part of the studied travertines is imprecisely dated. It may be an age equivalent of the Bešeňová travertine, the age of which is estimated to be between 780 and 350 ka, and the pollen assemblage suggests their formation in mild interglacial conditions (Gradziński *et al*., 2015). Travertines in Dudince in southern Slovakia are of a similar age, dated at ca. 301 ka (Vieira *et al*., 2023). This corresponds to MIS9. It is noteworthy that studies of speleothems in the Demänová Cave System indicate warm conditions in MIS9, but also only the weak glacial conditions of MIS10 (Błaszczyk and Hercman, 2022).

Post-sedimentary modification of spring-related carbonate

The entire complex of carbonates and intercalated siliciclastic deposits was laid down on a relatively flat area, which was fed with highly mineralised water by a perched spring and simultaneously with water, derived from the hinterland by surface drainage. Currently, Čerená Hill is disconnected from a surface drainage network. This suggests that, on the one hand, after the deposition of the youngest carbonate, the activity of the feeding spring ceased, and on the other, there was a reorganization of the surface drainage network. The former process was a result of entrenchments of the neighbouring valleys into older alluvial deposits and the Palaeogene rocks. Therefore, the neighbouring Ludrovianka and Komornícky streams, which border Čerená Hill from the west and east, respectively, must have deepened their valleys after ca. 208 ka.

The incision of neighbouring valleys resulted in the retreat and steepening of slopes, which caused the formation of the plateau-like relief of Čerená Hill. Such a kind of hill owes its formation to the existence of relatively erosion-prone Palaeogene layers at its base and well-cemented, flat-lying carbonate and underlying conglomerates at its top. The latter shielded some part of the base and determined the present plateau relief of the hill (see Wang *et al*., 2016). The slopes of the resistant carbonate geobody were shaped by mass-wasting processes (see Migoń *et al*., 2017). They resulted in a widening of fissures, cutting the carbonates and reaching the conglomerate bedrock near the edges of the hill (Vaškovský and Ložek, 1972). A crevice cave, measuring 27 m in length and 17 m in depth (for cave description see Hochmuth, 1993), located close to the eastern edge of the hill (Fig. 2), is another effect of these processes.

Spring-related carbonates were also subject to karst dissolution. This is evidenced by both the voids found in boreholes V-2 and V-6, with a vertical extent of up to a few metres (Fig. 2; Šubjak and Polášková, 1961), and a cavity, partly filled with speleothem calcite (Fig. 9). There are insufficient data to determine the time and conditions of these processes.

The proposed scenario of post-depositional modification of travertine implies that Čerená Hill cannot be regarded as a travertine mound, since mounds receive water from below during their growth, which determines their shape (Pentecost, 2005, p. 52–54). Conversely, the hill represents an erosional remnant of a travertine terrace, developed near a perched spring. The present plateau shape of the hill is mostly a result of denudation processes.

Geomorphic implications

Travertine, which can be isotopically dated, is used to estimate the age of underlying clastic deposits or fluvial terraces (Veldkamp *et al*., 2004; Ruszkiczay-Rüdiger *et al*., 2005; Wang *et al*., 2017). The Čerená carbonate was laid down on two large, gently inclined alluvial fans, deposited at the mouth of the river valley of the Ludrovianka Stream, a left-side tributary of the Váh River, to the adjacent part of the Liptov Basin (Droppa, 1972; Vaškovský and Ložek, 1972; Vaškovský, 1980). Droppa (1972) correlated the Quaternary sediments underlying the Čerená carbonate with the river terrace T-VI, which is stratigraphically ranged to glacial Günz-2. Later on, Vaškovský and Ložek (1972) as well as Vaškovský (1980) correlated the upper fan with terrace T-VI (Donau) and the lower fan with river terrace T-V (Günz).

Vitovič (2018) estimated the ages of the T-VI and T-V terraces to be approximately 1.3 and 1.04 Ma, respectively. Franko (2001) assumed that the Čerená carbonate formed during the Günz-Mindel interglacial (ca. 750–600 ka ago). The results of U-series dating and palaeomagnetic analyses collectively show that the deposition of carbonate started at ca. 300 ka. It was preceded by the cementation of gravel, which is bracketed between 0.5 and 1.2 Ma. The above data, though imprecise, appear to be in line with the proposed age of the underlying sediments. It can be borne in mind that the studied carbonate was deposited near a perched spring. Therefore, its age does not correspond to the age of the valley bottom (see the discussion in Ruszkiczay-Rüdiger *et al*., 2018). Furthermore, the periodic activity of the feeding spring may have caused the spring-related carbonate to significantly postdate the underlying sediments.

CONCLUSIONS

A comprehensive study of the complex of spring-related carbonates at Čerená Hill provides the following conclusions:

1. The carbonate complex was fed by deep-circulating water, containing geogenic CO_2, which is indicated by carbon stable isotopes. Its outflow supplied a marshy area, occasionally invaded by surface stream water. This is reflected in variations of the facies and their geochemical properties (i.e., $\delta^{13}C$ values and calcium carbonate content).
2. The presence of conglomerates at the base of the complex, and their absence from within it, suggests that during carbonate growth, the main fluvial channels were located at a greater distance from the carbonate complex, most likely in morphologically low areas.
3. The U-series dating results and palaeomagnetic data collectively show that the growth of the Čerená carbonate complex commenced ca. 300 ka and continued until ca. 200 ka. Growth during the warm climatic phases of the Pleistocene is also evidenced by the abundance of floral imprints and mollusc assemblages.
4. Considering the facies and geochemistry, the studied complex differs from either typical tufa or travertines, having attributes that are common to both of them. Therefore, the authors propose the term hybrid spring-related carbonates for such deposits.
5. The current shape of Čerená Hill is a result of post-sedimentary modification, which was initiated with disconnection from a supply of spring water. This modification included shaping by mass-wasting processes, resulting from the incision of the neighbouring valleys.

Acknowledgements

This study was financially supported by a grant from the Faculty of Geography and Geology under the Priority Research Area (Anthropocene) of the Strategic Programme Excellence Initiative at the Jagiellonian University, the Institutional Financing of the Institute of Geology, Czech Academy of Sciences No. RVO67985831, and Grant Project of the APVV Grant Agency NO. APVV-0625, New synthesis of relief evolution in Western Carpathians. We would like to acknowledge Katarzyna Maj-Szeliga and Michał Skiba, who helped with the X-Ray diffraction measurements. Robert Szczepanek is thanked for valuable suggestions on statistical calculations. Palaeomagnetic analyses were carried out by Kristýna Čížková, Jiří Petráček and Petr Petráček. We acknowledge the field assistance of Jan Sala, Miroslav Kudla, Pavol Papčo, Ján Soták and Juraj Šurka. The authors would like to thank reviewers Enrico Capezzuoli and Ladislav Vitovič, as well as the editors of *ASGP*, for their valuable comments, which greatly contributed to the improvement of this article.

REFERENCES

Aguillar, J., Oste, J. T. F., Erthal, M. M., Bó, P. F. D., Rodríguez-Berriguete, Á., Mendes, M. & Claes, H., 2024. Depositional and diagenetic processes in travertines: A comprehensive examination of Tocomar basin lithotypes, Northwest Argentina. *Journal of South American Earth Sciences*, 142: 104960.

Anczkiewicz, A. A., Danišík, M. & Środoń, J., 2015. Multiple low temperature thermochronology constraints on exhumation of the Tatra Mountains: New implication for the complex evolution of the Western Carpathians in the Cenozoic. *Tectonics*, 34: 2296–2317.

Arenas, C., Vázquez-Urbez, M., Auqué, L., Sancho, C., Osácar, C. & Pardo, G., 2014a. Intrinsic and extrinsic controls of spatial and temporal variations in modern fluvial tufa sedimentation: A thirteen-year record from a semi-arid environment. *Sedimentology*, 61: 90–132.

Arenas, C., Vázquez-Urbez, M., Pardo, G. & Sancho, C., 2014b. Sedimentology and depositional architecture of tufas deposited in stepped fluvial systems of changing slope: lessons from the Quaternary Añamaza valley (Iberian Range, Spain). *Sedimentology*, 61: 133–171.

Baker, A., Smart, P. L. & Edwards, R. L., 1996. Mass spectrometric of flowstone from Stump Cross Caverns and Lancaster Hole, Yorkshire: palaeoclimate implication. *Journal of Quaternary Sciences*, 11: 107–114.

Bella, P., Gradziński, M., Hercman, H., Leszczyński, S. & Nemec, W., 2021. Sedimentary anatomy and hydrological record of relic fluvial deposits in a karst cave conduit. *Sedimentology*, 68: 425–448.

Bisse, S. B., Ekomane, E., Eyong, J. T., Ollivier, V., Douville, E., Nganne, M. J. M. & Bitom, L. D., 2018. Sedimentological and geochemical study of the Bongongo and Ngol travertines located at the Cameroon Volcanic Line. *Journal of African Earth Sciences*, 143: 201–214.

Błaszczyk, M. & Hercman, H., 2022. Palaeoclimate in the Low Tatras of the Western Carpathians during MIS 11–6: Insights from multiproxy speleothem records. *Quaternary Science Reviews*, 275: 107290.

Błaszczyk, M., Hercman, H., Pawlak, J. & Szczygieł, J., 2020. Paleoclimatic reconstruction in the Tatra Mountains of the western Carpathians during MIS 9–7 inferred from a multiproxy speleothem record. *Quaternary Research*, 99: 290–304.

Brasier, A. T., 2011. Searching for travertines, calcretes and speleothems in deep time: Processes, appearances, predictions and the impact of plants. *Earth-Science Reviews*, 104: 213–239.

Brierley, G. J., Liu, K. & Crook, K. A., 1993. Sedimentology of coarse-grained alluvial fans in the Markham Valley, Papua New Guinea. *Sedimentary Geology*, 86: 297–324.

Brilli, M. & Giustini, F., 2023. Geochemical Stratigraphy of the Prima Porta Travertine Deposit (Roma, Italy). *Minerals*, 13: 789.

Brogi, A. & Capezzuoli, E., 2009. Travertine deposition and faulting: the fault-related travertine fissure-ridge at Terme S. Giovanni, Rapolano Terme (Italy). *International Journal of Earth Sciences*, 98: 931–947.

Brogi, A., Capezzuoli, E., Alçiçek, M. C. & Gandin, A., 2014. Evolution of a fault-controlled fissure-ridge type travertine deposit in the western Anatolia extensional province: the Çukurbağ fissure-ridge (Pamukkale, Turkey). *Journal of the Geological Society*, 171: 425–441.

Brogi, A., Capezzuoli, E., Aqué, R., Branca, M. & Voltaggio, M., 2010. Studying travertines for neotectonics investigations: Middle–Late Pleistocene syn-tectonic travertine deposition at Serre di Rapolano (Northern Apennines, Italy). *International Journal of Earth Sciences*, 99: 1383–1398.

Brogi, A., Capezzuoli, E., Buracchi, E. & Branca, M., 2012. Tectonic control on travertine and calcareous tufa deposition in a low-temperature geothermal system (Sarteano, Central Italy). *Journal of the Geological Society*, 169: 461–476.

Brogi, A., Capezzuoli, E., Moretti, M., Olvera-García, E., Matera, P. F., Garduno-Monroy, V. H. & Mancini, A., 2018. Earthquake-triggered soft-sediment deformation structures (seismites) in travertine deposits. *Tectonophysics*, 745: 349–365.

Capezzuoli, E., Gandin, A. & Pedley, M., 2014. Decoding tufa and travertine (fresh water carbonates) in the sedimentary record: The state of the art. *Sedimentology*, 61: 1–21.

Chadima, M. & Hrouda, F., 2006. Remasoft 3.0 – A user-friendly paleomagnetic data browser and analyser. *Travaux Géophysiques*, 27: 20–21.

Chafetz, H. S., Utech, N. M. & Fitzmaurice, S. P., 1991. Differences in the delta ^{18}O and delta ^{13}C signatures of seasonal laminae comprising travertine stromatolites. *Journal of Sedimentary Research*, 61: 1015–1028.

Cheng, H., Edwards, R. L., Hoff, J., Gallup, C. D., Richards, D. A. & Asmerom, Y., 2000. The half-lives of uranium-234 and thorium-230. *Chemical Geology*, 169: 17–33.

Claes, H., Degros, M., Soete, J., Claes, S., Kele, S., Mindszenty, A., Török, Á., El Desouky, H., Vanhaecke, F. & Swennen, R., 2017. Geobody architecture, genesis and petrophysical characteristics of the Budakalász travertines, Buda Hills (Hungary). *Quaternary International*, 437: 107-128.

Claes, H., Soete, J., Van Noten, K., El Desouky, H., Marques Erthal, M., Vanhaecke, F., Özkul, M. & Swennen, R., 2015. Sedimentology, three-dimensional geobody reconstruction and carbon dioxide origin of Pleistocene travertine deposits in the Ballık area (south-west Turkey*). Sedimentology*, 62: 1408–1445.

Collinson, J. D., 1986. Alluvial sediments. In: Reading, H. G. (ed.), *Sedimentary Environments: Processes, Facies and Stratigraphy*. Blackwell, Oxford, pp. 688.

Constantin, S., Bojar, A-V., Lauritzen, S. E. & Lundberg, J., 2007. Holocene and Late Pleistocene climate in the sub-Mediterranean continental environment: A speleothem record from Poleva Cave (Southern Carpathians, Romania). *Palaeogeography, Palaeoclimatology, Palaeoecology*, 243: 322–338.

Cornides, I. & Kecskés, Á., 1982. Deep-seated carbon dioxide in Slovakia: Additional comments on the problem of its origin. *Geologický Zbornik Geologica Carpathica*, 33: 183–190.

Cosford, J., Qing, H., Yuan, D., Zhang, M., Holmden, C., Patterson, W. & Hai, C., 2008. Millennial-scale variability in the Asian monsoon: Evidence from oxygen isotope records from stalagmites in southeastern China. *Palaeogeography, Palaeoclimatology, Palaeoecology*, 266: 3–12.

Croci, A., Della Porta, G. & Capezzuoli, E., 2016. Depositional architecture of a mixed travertine-terrigenous system in a fault-controlled continental extensional basin (Messinian, Southern Tuscany, Central Italy). *Sedimentology*, 332: 13–39.

Crossey, L. J., Fischer, T. P., Patchett, P. J., Karlstrom, K. E., Hilton, D. R., Newell, D. L., Huntoon, P., Reynolds, A. & De Leeuw, G. A., 2006. Dissected hydrologic system at the Grand Canyon: Interaction between deeply derived fluids and plateau aquifer waters in modern springs and travertine. *Geology*, 34: 25–28.

Cruz, Jr., F. W., Burns, S. J., Karmann, I., Sharp, W. D., Vulle, M., Cardaso, A. O., Ferrari, J. A., Dias, P. L. S. & Vlana Jr., O., 2005. Insolation-driven changes in atmospheric circulation over the past 116,000 years in subtropical Brazil. *Nature*, 434: 63–65.

De Boever, E., Foubert, A., Lopez, B., Swennen, R., Jaworowski, C., Özkul, M. & Virgone, A., 2017. Comparative study of the Pleistocene Cakmak quarry (Denizli basin, Turkey) and modern mammoth hot springs deposits (Yellowstone National Park, USA). *Quaternary International*, 437: 129–146.

De Filippis, L., Faccenna, C., Billi, A., Anzalone, E., Brilli, M., Soligo, M. & Tuccimei, P., 2013. Plateau versus fissure ridge travertines from Quaternary geothermal springs of Italy and Turkey: Interactions and feedbacks between fluid discharge, paleoclimate, and tectonics. *Earth-Science Reviews*, 123: 35–52.

Della Porta, G., 2015. Carbonate build-ups in lacustrine, hydrothermal and fluvial settings: comparing depositional geometry, fabric types and geochemical signature. In: Bosence, D. W. J., Gibbons, K. A., Le Heron, D. P., Morgan, W. A., Pritchard, T. & Vining, B. A. (eds), *Microbial Carbonates in Space and Time: Implications for Global Exploration and Production*. *Geological Society Special Publications*, 418: 17–68.

Della Porta, G., Capezzuoli, E. & De Bernardo, A., 2017. Facies character and depositional architecture of hydrothermal travertine slope aprons (Pleistocene, Acquasanta Terme, Central Italy). *Marine and Petroleum Geology*, 87: 171–187.

Dorale, J. A., Gonzalez, L. A., Reagan, M. K., Pickett, D., Murell, M. T. & Baker, R.G., 1992. A High-Resolution Record of Holocene Climate Change in Speleothem Calcite from Cold Water Cave, Northeast Iowa. *Science*, 258: 1625–1630.

Droppa, A., 1964. Die Erforschung der Váh-terrassen im mittleren Teile des Kessels Liptovská kotlina. *Geografický časopis*, 16: 313–325. [In Slovak, with German summary.]

Droppa, A., 1972. Výskum riečnych terás v okolí Ružomberka. In: Kufčák, E. (ed.), *Liptov 2*. Vlastivedný zborník. Martin (Osveta), pp. 11–25. [In Slovak.]

Dykoski, C. A., Edwards, R. L., Cheng, H., Yuan, D., Cai, Y., Zhang, M., Lin, Y., Qing, J., An, Z. & Revenaugh, J., 2005. A high-resolution, absolute-dated Holocene and deglacial Asian monsoon record from Dongge Cave, China. *Earth and Planetary Letters*, 233: 71–86.

Erthal, M. M., Capezzuoli, E., Mancini, A., Claes, H., Soete, J. & Swennen, R., 2017. Shrub morpho-types as indicator for the water flow energy-Tivoli travertine case (Central Italy). *Sedimentary Geology*, 347: 79–99.

Faccenna, C., Soligo, M., Billi, A., De Filippis, L., Funiciello, R., Rossetti, C. & Tuccimei, P., 2008. Late Pleistocene depositional cycles of the Lapis Tiburtinus travertine (Tivoli, central Italy): possible influence of climate and fault activity. *Global and Planetary Change*, 63: 299–308.

Fairchild, I. J. & Baker, A., 2012. *Speleothem science: from process to past environments*. John Wiley & Sons, Oxford, 448 pp.

Fisher, R., 1953. Dispersion on a sphere. *Proceedings of the Royal Society of London*, Series A, 217: 295–305.

Fleitmann, D., Burns, S. J., Neff, U., Mudelsee, M., Mangini, A. & Matter, A., 2004. Palaeoclimatic interpretation of high-resolution oxygen isotope profiles derived from annually laminated speleothems from Southern Oman. *Quaternary Science Reviews*, 23: 935–945.

Ford, T. D. & Pedley, H. M., 1996. A review of tufa and travertine deposits of the world. *Earth-Science Reviews*, 41: 117–175.

Franko, O., 2001. Origin and development of mineral and thermal waters of Slovakia in space and time from the view of the age of travertines and 18O, H and 14C isotopes. *Podzemná voda,* 7: 26–44. [In Slovak, with English summary.]

Franko, O. & Šivo, A., 1999. Relative, geological and absolute age of the geothermal waters in north Slovakia. *Proceedings of XXIX Congress of IAH „Hydrogeology and land use management"*. Publ. Slovak IAH, Bratislava, pp. 681–684.

Freytet, P. & Verrecchia, E. P., 1998. Freshwater organisms that build stromatolites: a synopsis of biocrystallization by prokaryotic and eukaryotic algae. *Sedimentology*, 45: 535–563.

Frisia, S., 2015. Microstratigraphic logging of calcite fabrics in speleothems as tool for palaeoclimate studies. *International Journal of Speleology*, 44: 1–16.

Gandin, A. & Capezzuoli, E., 2014. Travertine Distinctive depositional fabrics of carbonates from thermal spring system. *Sedimentology*, 61: 264–290.

García-García, F., Pla-Pueyo, S., Nieto, L. M. & Viseras, C., 2014. Sedimentology of geomorphologically controlled Quaternary tufas in a valley in southern Spain. *Facies*, 60: 53–72.

Gierlowski-Kordesch, E. H., 2010. Lacustrine carbonates. In: Alonso-Zarza, A. M. & Tanner, L. H. (eds), *Carbonates in Continental Settings: Facies, Environments and Processes. Developments in Sedimentology*, 61: 1–102.

Gori, F., Damato, A., Anselmi, M., Baneschi, I., Barberio, M. D., Barbieri, M., Billi, A., Boschetti, T., Curzi, M., Lucianetti, G., Salvadori, M., Sciarra, A. & Petitta, M., 2025. Combined impact of climate and seismic activity on groundwater hydrogeochemistry in the Eastern Southern Alps, Italy. *Science of the Total Environment*, 1004: 180771.

Gradziński, M., 2010. Factors controlling growth of modern tufa: results of a field experiment. In: Pedley, H. M. & Rogerson, M. (eds), *Tufas and Speleothems: Unravelling the Microbial and Physical Controls*. *Geological Society Special Publications*, 336: 143–191.

Gradziński, M., Chmiel, M. J., Lewandowska, A. & Michalska-Kasperkiewicz, B., 2010. Siliciclastic microstromatolites in a sandstone cave: role of trap ping and binding of detrital particles in formation of cave deposits. *Annales Societatis Geologorum Poloniae*, 80: 303–314.

Gradziński, M., Duliński, M., Hercman, H., Stworzewicz, E., Holúbek, P., Rajnoga, P., Wróblewski, W. & Kováčová, M., 2008. Facies and age of travertines from Spiš and Liptov regions (Slovakia) – preliminary results. *Slovenský kras*, 46: 31–40.

Gradziński, M., Hercman, H., Jaśkiewicz, M. & Szczurek, S., 2013. Holocene tufa in the Slovak Karst: facies, sedimentary environments and depositional history. *Geological Quarterly*, 57: 769–788.

Gradziński, M., Hercman, H. & Staniszewski, K., 2014b. Middle Pleistocene carbonate-cemented colluvium in southern Poland: Its depositional processes, diagenesis and regional palaeoenvironmental significance. *Sedimentary Geology*, 306: 24–35.

Gradziński, M., Wróblewski, W. & Bella, P., 2015. Cenozoic freshwater carbonates of the Central Carpathians (Slovakia): facies, environments, hydrological control and depositional history. In: Haczewski, G. (ed.), *Guidebook for field trips accompanying 31st IAS Meeting of Sedimentology held in Kraków on 22nd-25th of June 2015*. Polish Geological Society, Kraków, pp. 217–245.

Gradziński, M., Wróblewski, W., Duliński, M. & Hercman, H., 2014a. Earthquake-affected development of a travertine ridge. *Sedimentology*, 61: 238–263.

Gross, P., Köhler, E., Papšová, J. & Snopková, P., 1980. Geológia a stratigrafia sedimentov vnútrokarpatského paleogénu. In: Gross, P. & Köhler, E. (eds), *Geológia Liptovskej kotliny*. Geologický ústav Dionýza Štúra, Bratislava, pp. 22–72. [In Slovak.]

Gross, P., Köhler, E. & Samuel, O., 1984. A new lithostratigraphical division of the Inner-Carpathian Paleogene. *Geologické práce, Správy,* 81: 103–117. [In Slovak, with English summary.]

Gross, P. (ed), Vaškovský, I. & Halouzka, R., 1979: G*eologická mapa Liptovskej kotliny 1:50 000*. Geologický ústav Dionýza Štúra, Bratislava.

Guo, L. & Riding, R., 1998. Hot-spring travertine facies and sequences, Late Pleistocene, Rapolano Terme, Italy. *Sedimentology*, 45: 163–180.

Guo, L. & Riding, R., 1999. Rapid facies changes in Holocene fissure ridge hot spring travertines, Rapolano Terme, Italy. *Sedimentology*, 46: 1145–1158.

Hancock, P. L., Chalmers, R. M. L., Altunel, E. & Cakir, Z., 1999. Travitonics: using travertines in active fault studies. *Journal of Structural Geology*, 21: 903–916.

Hochmuth, Z., 1993. Krasové javy masívu Salatína v Nízkych Tatrách. *Spravodaj Slovenskej speleologickej spoločnosti*, 24: 7–12. [In Slovak.]

Hoefs, J., 2018. *Stable Isotope Geochemistry*. Springer, Cham, 437 pp.

Holden, N. E., 1990. Total half-lives for selected nuclides. *Pure and Applied Chemistry*, 62: 941–958.

Hynie, O., 1963. *Hydrogeologie ČSSR, II, Minerální vody*. Nakladatelství Československé Akademie Véd, Praha, 797 pp. [In Czech.]

Ivan, Ľ., 1943. Výskyty travertínov na Slovensku. *Práce Štátneho geologického ústavu*, 9: 1–71. [In Slovak.]

Ivanovich, M. & Harmon, R. S., 1992. Uranium-series Disequilibrium: Application to Earth, Marine and Environmental Sciences. Clarendon Press, Oxford. Oxford, 910 pp.

Jackson, M. L., 1969. *Soil Chemical Analysis: Advanced Course*. Edition 2. Madison, Wisconsin, USA, 895 pp.

Jaffey, A. H., Flynn, K. F., Glendenin, L. E., Bentley, W. C. & Essling, A. M., 1971. Precision measurement of half-lives and specific activities of U-235 and U-238. *Physical Review C*, 4: 1889–1905.

Janssens, N., Capezzuoli, E., Claes, H., Muchez, P., Yu, T. L., Shen, C.-C., Ellam, R. M. & Swennen, R., 2020. Fossil travertine system and its palaeofluid provenance, migration and evolution through time: Example from the geothermal area of Acquasanta Terme (Central Italy). *Sedimentary Geology*, 398: 105580.

Jelínek, V., 1966. A high sensitivity spinner magnetometer. *Studia Geophysica et Geodaetica*, 10: 58–78.

Jelínek, V., 1973. Precision A.C. bridge set for measuring magnetic susceptibility and its anisotropy. *Studia Geophysica et Geodaetica*, 17: 36–48.

Jones, B. & Renaut, R. W., 2010. Calcareous spring deposits in continental settings. *Developments in Sedimentology*, 61: 177–224.

Kaufman, A., 1993. An evaluation of several methods for determining ^{230}Th/U ages in impure carbonates. *Geochimica et Cosmochimica Acta*, 57: 2303–2317.

Kaufman, A. & Brocker, W.S., 1965. Comparison of ^{230}Th and ^{14}C ages for carbonate materials from Lakes Lahontans and Bonneville. *Journal of Geophysical Research*, 70: 4039–4054.

Kele, S., Demény, A., Siklósy, Z., Németh, T., Tóth, M. & Kovács, M. B., 2008. Chemical and stable isotope composition of recent hot-water travertines and associated thermal waters, from Egerszalók, Hungary: Depositional facies and non-equilibrium fractionation. *Sedimentary Geology*, 211: 53–72.

Kele, S., Özkul, M., Fórizs, I., Gökgöz, A., Baykara, M. O., Alçiçek, M. C. & Németh, T., 2011. Stable isotope geochemical study of Pamukkale travertines: new evidences of low-temperature non-equilibrium calcite-water fractionation. *Sedimentary Geology*, 238: 191–212.

Kirschvink, J. L., 1980. The least-squares line and plane and the analysis of palaeomagnetic data. *Geophysical Journal Royal Astronomical Society*, 62: 699–718.

Kovanda, J., 1971. Kvartérní vápence Československa. *Sbornik Geologických Véd Antropozoikum*, A7, pp. 7–256. [In Czech, with English summary.]

Králiková, S., Vojtko, R., Sliva, L., Minár, J., Fügenschuh, B., Kováč, M. & Hók, J., 2014. Cretaceous–Quaternary tectonic evolution of the Tatra Mts (Western Carpathians): Constraints from structural, sedimentary, geomorphological, and fission track data. *Geologica Carpathica*, 65: 307–326.

Kucharič, L. U., Bodiš, D., Panák, D., Liščák, P. & Božíková, J., 2015. A contribution of CO_2 released from mineral springs into overall volume of annual CO_2 emissions in the Slovak Republic. *Environmental Earth Sciences*, 73: 231–238.

Leśniak, P. M., 1998. Origin of carbon dioxide and evolution of CO_2-rich waters in the West Carpathians, Poland. *Acta Geologica Polonica*, 48: 343–366.

Li, H. C., Ku, T. L., You, C. F., Cheng, H., Edwards, R. L., Ma, Z. B., Tsai, W. S. & Li, M. D., 2005. ^{87}Sr/^{86}Sr and Sr/Ca in speleothems for paleoclimate reconstruction in Central China between 70 and 280 kyr age. *Geochimica et Cosmochimica Acta*, 69: 3933–3947.

Lin, J. C., Broecker, W. S., Anderson, R. F., Hemming, S., Rubenstone, J. L. & Bonani, G., 1996. New Th-230/U and C-14 ages from Lake Lahontan carbonates, Nevada, USA and a discussion of the origin of initial thorium. *Geochimica et Cosmochimica Acta*, 60: 2817–2832.

Linge, H., Baker, A., Andersson, C. & Lauritzen, S. E., 2009. Variability in luminescent lamination and initial ^{230}Th/^{232}Th activity ratios in a late Holocene stalagmite from northern Norway. *Quaternary Geochronology*, 4: 181–192.

Liu, Z., Zhang, M., Li, Q. & You, S., 2003. Hydrochemical and isotope characteristics of spring water and travertine in the Baishuitai area (SW China) and their meaning for paleoenvironmental reconstruction. *Environmental Geology*, 44: 698–704.

Ložek, V., 1961. Travertines. *Instytut Geologiczny, Prace,* 34: 81–86.

Ložek, V., 1964. Quartärmollusken der Tschechoslowakei. *Rozpravy Ústředního ústavu geologického* 31, Praha, 374 pp.

Ložek, V., 1973. *Příroda ve čtvrtohorách*. Akademia, Praha, 372 pp. [In Czech.]

Lundberg, J., Brewer-Carias, C. & McFarlane, D. A., 2010. Preliminary results from U-Th dating of glacial-interglacial deposition cycles in a silica speleothems from Venezuela. *Quaternary Research*, 74: 113–120.

Luo, L., Capezzuoli, E., Vaselli, O., Wen, H., Lazzaroni, M., Lu, Z., Meloni, F. & Kele, S., 2021. Factors governing travertine deposition in fluvial systems: The Bagni San Filippo (central Italy) case study. *Sedimentary Geology*, 426: 106023.

Maheľ, M. & Buday, T., 1968. *Regional Geology of Czechoslovakia. Part II. The West Carpathians*. Geological Survey of Czechoslovakia, Academia, Praha, 723 pp.

Man, O., 2008. On the identification of magnetistratigraphic polarity zones. *Studia Geophysica at Geodaetica*, 52: 173–186.

Mancini, A., Della Porta, G., Swennen, R. & Capezzuoli, E., 2021. 3D reconstruction of the Lapis Tiburtinus (Tivoli, Central Italy): The control of climatic and sea-level changes on travertine deposition. *Basin Research*, 33: 2605–2635.

Migoń, P., Duszyński, F. & Goudie, A., 2017. Rock cities and ruiniform relief: Forms – processes – terminology. *Earth-Science Reviews*, 171: 78–104.

Mohammadi, Z., Claes, H., Capezzuoli, E., Mozafari, M., Soete, J., Aratman, C. & Swennen, R., 2020. Lateral and vertical variations in sedimentology and geochemistry of sub-horizontal laminated travertines (Çakmak quarry, Denizli Basin, Turkey). *Quaternary International*, 540: 146–168.

Mors, R. A., Astini, R. A. & Gomez, F. J., 2019. Coexisting active travertines and tufas in the southeastern border of the Puna plateau. *Sedimentary Geology*, 389: 200–217.

Mystkowski, K., 1999. ClayLab, a computer program for processing and interpretation of X-ray diffractograms of clays. *Conference of European Clay Groups Association, EUROCLAY 1999*. Book of abstracts, Krakow, Poland, pp. 114–115

Onac, B. P., Constantin, S., Lundberg, J. & Lauritzen, S. E., 2002. Isotopic climate record in a Holocene stalagmite from Ursilor Cave (Romania). *Journal of Quaternary Sciences*, 17: 319–327.

Özkul, M., Gökgöz, A., Kele, S., Baykara, M. O., Shen, C., Chang, Y., Kaya, A., Hançer, M., Aratman, C., Akin, T. & Örü, Z., 2014. Sedimentological and geochemical characteristics of a fluvial travertine: A case from the eastern Mediterranean region. *Sedimentology*, 61: 291–318.

Özkul, M., Kele, S., Gökgöz, A., Shen, C. C., Jones, B., Baykara, M. O., Fórizs, I., Németh, T., Chang, Y.-W. & Alçiçek, M. C.,

2013. Comparison of the Quaternary travertine sites in the Denizli extensional basin based on their depositional and geochemical data. *Sedimentary Geology*, 294: 179–204.

Panichi, C. & Tongiorgi, E., 1976. Carbon isotopic composition of CO_2 from springs, fumaroles, mofettes and travertines of central and southern Italy: a preliminary prospection method of geothermal area. In: *Proceedings of the 2nd United Nations Symposium on the Development and Use of Geothermal Energy, 20–29 May 1975*. San Francisco, U.S.A., pp. 815–825.

Pedley, M., 1990. Classification and environ mental models of cool freshwater tufas. *Sedimentary Geology*, 68: 143–154.

Pedley, M., 2009. Tufas and travertines of the Mediterranean region: a testing ground for freshwater carbonate concepts and developments. *Sedimentology*, 56: 221–246.

Pedley, M., 2014. The morphology and function of thrombolitic calcite precipitating biofilms: A universal model derived from freshwater mesocosm experiments. *Sedimentology*, 61: 22–40.

Pedley, M., Rogerson, M. & Middleton, R., 2009. Freshwater calcite precipitates from in vitro mesocosm flume experiments: a case for biomediation of tufas. *Sedimentology*, 56: 511–527.

Pentecost, A., 1995. The Quaternary travertine deposits of Europe and Asia Minor. *Quaternary Science Reviews,* 14: 1005–1028.

Pentecost, A., 2005. *Travertine*. Springer, Berlin, 445 pp.

Pivko, D., 2021. A review of Slovak travertine and tufa facies and their environment. *Acta Geologica Slovaca*, 13: 129–166.

Pivko, D. & Vojtko, R., 2021. A review of travertines and tufas in Slovakia: Geomorphology, environments, tectonic pattern, and age distribution. *Acta Geologica Slovaca*, 13: 49–78.

Plašienka, D., 2008. The Western Carpathians. In: McCann, T. (ed.), *The Geology of central Europe. Volume 2: Mesozoic and Cenozoic*. The Geological Society, London, pp. 1181–1217.

Plašienka, D., 2018. The Carpathian Klippen Belt and types of its klippen – an attempt at a genetic classification. *Mineralia Slovaca*, 50: 1–24.

Povinec, P. P., Franko, O., Šivo, A., Richtárikova, M., Breier, R., Aggarwal, P. K. & Araguás-Araguás, L., 2010. Spatial radiocarbon and stable carbon isotope variability of mineral and thermal waters in Slovakia. *Radiocarbon*, 52: 1056–1067.

Priewisch, A., Crossey, L. J., Karlstrom, K. E., Polyak, V. J., Asmerom, Y., Nereson, A. & Ricketts, J. W., 2014. U-series geochronology of large-volume Quaternary travertine deposits of the southeastern Colorado Plateau: Evaluating episodicity and tectonic and paleohydrologic controls. *Geosphere*, 10: 401–423.

Příhoda, K., Krs, M., Pešina, B. & Bláha, J., 1989. MAVACS – a new system of creating a non-magnetic environment for palaeomagnetic studies. *Cuaderna Geologia Ibérica*, 12: 223–250.

Rainey, D. K. & Jones, B., 2007. Rapid cold water formation and recrystallization of relict bryophyte tufa at the Fall Creek cold springs, Alberta, Canada. *Canadian Journal of Earth Sciences*, 44: 889–909.

Rainey, D. K. & Jones, B., 2009. Abiotic versus biotic controls on the development of the Fairmont Hot Springs carbonate deposit, British Columbia, Canada. *Sedimentology*, 56: 1832–1857.

Riding, R., 1991. *Calcareous Algae and Stromatolites*. Springer, Berlin, Heidelberg, 571 pp.

Rihs, S., Condomines, M. & Sigmarsson, O., 2000. U, Ra and Ba incorporation during precipitation of hydrothermal carbonates: Implications for ^{226}Ra-Ba dating of impure travertines. *Geochimica et Cosmochimica Acta*, 64: 661–671.

Rodríguez-Berriguete, Á., 2020. Early diagenetic features in Holocene travertine and tufa from a volcanic setting (Azuaje, Gran Canaria, Spain). *Facies*, 66: 17.

Rodríguez-Berriguete, Á. & Alonso-Zarza, A. M., 2019. Controlling factors and implications for travertine and tufa deposition in a volcanic setting. *Sedimentary Geology*, 381: 13–28.

Rodríguez-Berriguete, Á., Alonso-Zarza, A. M. & Martín-García, R., 2017. Diagenesis of continental carbonate country rocks underlying surficial travertine spring deposits. *Quaternary International*, 437: 4–14.

Rodríguez-Berriguete, Á., Camuera, J. & Alonso-Zarza, A. M., 2022. Carbonate tufas as archives of climate and sedimentary dynamic in volcanic settings, examples from Gran Canaria (Spain). *Sedimentology*, 69: 199–218.

Ruszkiczay-Rüdiger, Z., Csillag, G., Fodor, L., Braucher, R., Novothny, Á., Thamó-Bozsó, E., Virág, A., Pazonyi, P., Timár, G. & Aster Team, 2018. Integration of new and revised chronological data to constrain the terrace evolution of the Danube River (Gerecse Hills, Pannonian Basin). *Quaternary Geochronology*, 48: 148–170.

Ruszkiczay-Rüdiger, Z., Fodor, L., Bada, G., Leél-Össy, S., Horváth, E. & Dunai, T. J., 2005. Quantification of Quaternary vertical movements in the central Pannonian Basin: a review of chronologic data along the Danube River, Hungary. *Tectonophysics*, 410: 157–172.

Sala, P., 2016. Facje trawertynów na stanowisku Čerená (Kotlina Liptowska, Słowacja). Unpublished MSc. Thesis, Jagiellonian University, 47 pp. [In Polish, with English summary.]

Sanders, D., Wertl, W. & Rott, E., 2011. Spring-associated limestones of the Eastern Alps: overview of facies, deposystems, minerals, and biota. *Facies*, 57: 395–416.

Scalera, F., Mancini, A., Capezzuoli, E., Claes, H. & Swennen, R., 2022. The role of tectonic activity, topographic gradient and river flood events in the Testina travertine (Acque Albule Basin, Tivoli, Central Italy). *The Depositional Record*, 8: 266–291.

Schwarcz, H. P., 1980. Absolute age determinations of archaeological sites by uranium dating of travertines. *Archaeometry*, 22: 3–24.

Shiraishi, F., Akimoto, T., Tomioka, N., Motai, S. & Takahashi, Y., 2023. Formation processes of paper-thin raft and coated bubble: Calcium carbonate deposition at gas–water interface. *Sedimentary Geology,* 456: 106514.

Shiraishi, F., Hanzawa, Y., Nakamura, Y., Eno, Y., Morikawa, A., de Mattos, R. F., Asada, J., Cury, L. F. & Bahniuk, A. M., 2022. Abiotic and biotic processes controlling travertine deposition: Insights from eight hot springs in Japan. *Sedimentology*, 69: 592–623.

Shiraishi, F., Morikawa, A., Kuroshima, K., Amekawa, S., Yu, T.-L., Shen, C.-C., Kakizaki, Y., Kano, A., Asada, J. & Bahniuk, A. M., 2020. Genesis and diagenesis of travertine, Futamata hot spring, Japan. *Sedimentary Geology*, 405: 105706.

Shiraishi, F., Okumura, T., Takahashi, Y. & Kano, A., 2010. Influence of microbial photosynthesis on tufa stromatolite formation and ambient water chemistry, SW Japan. *Geochimica et Cosmochimica Acta*, 74: 5289–5304.

Singer, B. S., 2014. A Quaternary geomagnetic instability time scale. *Quaternary Geochronology*, 21: 29–52.

Słowakiewicz, M., Borkowski, A., Perri, E., Działak, P., Tagliasacchi, E., Gradziński, M., Kele, S., Reuning, L., Kibblewhite, T., Whitaker, F., Reid, R. P. & Tucker, M. E., 2024. Biofilms in modern $CaCO_3$-supersaturated freshwater environments reveal viral proxies. *Scientific Reports*, 14: 25889.

Słowakiewicz, M., Perri, E., Tagliasacchi, E., Działak, P., Borkowski, A., Gradziński, M., Kele, S. & Tucker, M. E., 2023. Viruses participate in the organomineralization of travertines. *Scientific Reports*, 13: 11663.

Smolíková, L. & Ložek, V., 1962. Zur Altersfrage der mitteleuropäischen Terre Calais. *Eiszeitalter und Gegenwart*, 13: 157–177. [In German.]

Soták, J., 1998. Sequence stratigraphy approach to the Central Carpathian Paleogene (Eastern Slovakia): eustasy and tectonics as controls of deep-sea fan deposition. *Slovak Geological Magazine*, *4*: 185–190.

Środoń, J., 2006. Identification and quantitative analysis of clay minerals. In: Bergaya, F., Theng, B. K. G. & Lagaly, G. (eds), *Handbook of Clay Science*. *Developments in Clay Science, Vol. 1*. Elsevier, Amsterdam, pp. 765–787.

Suarez-Gonzalez, P., Benito, M. I., Quijada, I. E., Mas, R. & Campos-Soto, S., 2019. Trapping and binding: A review of the factors controlling the development of fossil agglutinated microbialites and their distribution in space and time. *Earth-Science Reviews*, 194: 182–215.

Šubjak, K. & Polášková, M., 1961. *Záverečná správa o výpočte zásob travertínov Ludrová, Bešeňová*. Manuscript, Geofond, Bratislava, 46 pp. [In Slovak.]

Tagliasacchi, E. & Kayseri-Özer, M. S., 2020. Multidisciplinary approach for palaeoclimatic signals of the non-marine carbonates: The case of the Sarıkavak tufa deposits (Afyon, SW-Turkey). *Quaternary International*, 544: 41–56.

Toker, E., 2017. Quaternary fluvial tufas of Sarıkavak area, southwestern Turkey: Facies and depositional systems. *Quaternary International*, 437: 37–50.

Toker, E., Kayseri-Özer, M. S., Özkul, M. & Kele, S., 2015. Depositional system and palaeoclimatic interpretations of Middle to Late Pleistocene travertines: Kocabaş, Denizli, south-west Turkey. *Sedimentology*, 62: 1360–1383.

Török, Á., Claes, H., Brogi, A., Liotta, D., Tóth, Á., Mindszenty, A., Kudó, I., Kele, S., Huntington, K., Shen, C.-C. & Swennen, R., 2019. A multi–methodological approach to reconstruct the configuration of a travertine fissure ridge system: The case of the Cukor quarry (Süttő, Gerecse Hills, Hungary). *Geomorphology*, 345: 106836.

Török, Á., Mindszenty, A., Claes, H., Kele, S., Fodor, L. & Swennen, R., 2017. Geobody architecture of continental carbonates: "Gazda" travertine quarry (Süttő, Gerecse Hills, Hungary). *Quaternary International*, 437: 164–185.

Van Noten, K., Topal, S., Baykara, M. O., Özkul, M., Claes, H., Aratman, C. & Swennen, R., 2019. Pleistocene-Holocene tectonic reconstruction of the Ballık travertine (Denizli Graben, SW Turkey): (De)formation of large travertine geobodies at intersecting grabens. *Journal of Structural Geology*, 118: 114–134.

Varejão, G. F., Alonso, G. E., Athayde, G. B., Bahniuk Rumbelsperger, A. M. & Cury, L. F., 2025. Facies stacking and lateral variability of travertines from the Quaternary Vega Botijuela, Salar de Antofalla Basin, Argentina. *Sedimentology*, 72: 533–568.

Vaškovský, I., 1980. Geológia kvartérnych sedimentov. In: Gross, P. & Köhler, E. (eds), *Geológia Liptovskej kotliny*. Geologický ústav Dionýza Štúra, Bratislava, pp. 96–115. [In Slovak.]

Vaškovský, I. & Ložek, V., 1972. To the Quaternary stratigraphy in the western part of the basin Liptovská kotlina. *Geologické práce*, *Správy*, 59: 101–140.

Vázquez-Urbez, M., Arenas, C. & Pardo, G., 2012. A sedimentary facies model for stepped, fluvial tufa system in the Iberian Range (Spain): the Quaternary Piedra and Mesa valleys. *Sedimentology*, 59: 502–526.

Veldkamp, A., Kroonenberg, S., Heijnis, H. & van den Berg van Saparoea, R., 2004. The suitability of dated travertines as a record of fluvial incision: Allier (France) floodplain dynamics during the Late quaternary. *Quaternaire*, 15: 159–165.

Vieira, D. S. C., Pivko, D., Rinyu, L., Palcsu, L., Kiss, G. I., Hu, H.-M., Shen, C.-C. & Kele, S., 2023. Age and Depositional Temperature of Quaternary Travertine Spring Mounds from Slovakia. *Minerals*, 13: 794

Vitovič, L., 2018. Riečne terasy a intenzita erózie Váhu v Liptovskej kotline. In: Galamboš, M. (ed.), *Študentská vedecká konferencia PriF UK 2018. Zborník recenzovaných príspevkov*. Univerzita Komenského, Bratislava, pp. 1345–1350. [In Slovak.]

Vitovič, L., 2020. Analysis of fluvial systems in the vicinity of Bežan Hill (Liptovská kotlina Basin, Western Carpathians). *Geografické informácie*, 24: 44–59.

Vitovič, L. & Minár, J., 2018. Morphotectonic analysis for improvement of neotectonic subdivision of the Liptovská kotlina Basin (Western Carpathians). *Geographical Journal*, 70: 197–216.

Vitovič, L., Minár, J., Bella, P. & Littva, J., 2022. Polygenetic relief in the foreland of glacially sculptured mountains – Podtatranská kotlina Basin. In: Lehotský, M. & Boltižiar, M. (eds), *Landscapes and Landforms of Slovakia*. Springer Cham, pp. 163–188.

Vitovič, L., Minár, J. & Pánek, T., 2021. Morphotectonic configuration of the Podtatranská Kotlina Basin and its relationship to the origin of the Western Carpathians. *Geomorphology*, 394: 107963.

Wang, Y. J., Cheng, H., Edwards, R. L., An, Z. S., Wu, J. Y., Shen, C. C. & Dorale, J. A., 2001. A high-resolution absolute-dated Late Pleistocene monsoon record from Hulu Cave. *Science*, 294: 2345–2348.

Wang, Z., Meyer, M. C., Gliganic, L. A., Hoffmann, D. L. & May, J. H., 2017. Timing of fluvial terrace formation and concomitant travertine deposition in the upper Sutlej River (Tirthapuri, southwestern Tibet) and paleoclimatic implications. *Quaternary Science Reviews*, 169: 357–377.

Wang, Z., Meyer, M. C. & Hoffmann, D. L., 2016. Sedimentology, petrography and early diagenesis of a travertine–colluvium succession from Chusang (southern Tibet). *Sedimentary Geology*, 342: 218–236.

Wright, V. P., 2012. Lacustrine carbonates in rift settings: the interaction of volcanic and microbial processes on carbonate deposition. In: Garland, J., Neilson, J. E., Laubach, S. E. & Whidden, K. J. (eds), *Advances in carbonate exploration and reservoir analysis. Geological Society Special Publications*, 370: 39–47

Wright, V. P., 2022. The mantle, CO_2 and the giant Aptian chemogenic lacustrine carbonate factory of the South Atlantic: Some carbonates are made, not born. *Sedimentology*, 69: 47–73.

Wróblewski, W., Bella, P., Drewnik, M., Duliński, M., Gradziński, M., Motyka, J., Nęcki, J. & Sala, P., 2024. Mixing of endogenous CO_2 and meteoric H_2O causes extremely efficient carbonate dissolution. *Science of the Total Environment*, 936: 173347.

Xia, Q., Zhao, J. X. & Collerson, K. D., 2001. Early-Mid Holocene climatic variations in Tasmania, Australia: multi-proxy records in a stalagmite from Lynds Cave. *Earth and Planetary Letters*, 194: 177–187.

Zhao, J. X., Wang, Y. J., Collerson, K. D. & Gagan, M. K., 2003. Speleothem U-series dating of semi-synchronous climate oscillations during the last deglaciation. *Earth and Planetary Letters*, 216: 155–161.

Zieliński, T., 2014. *Sedymentologia. Osady rzek i jezior*. Wydawncitwo Naukowe UAM, Poznań, 594 pp. [In Polish.]

Zupan Hajna, N., Mihevc, A., Pruner, P. & Bosák, P., 2008. Palaeomagnetism and Magnetostratigraphy of Karst Sediments in Slovenia. *Carsologica*, 8: 1–266.